The Thesis Committee for Anine Oehlenschlaeger Pedersen
Certifies that this is the approved version of the following thesis:

Dune Behavior in a Multidirectional Wind Regime: White Sands Dune Field, New Mexico

APPROVED BY
SUPERVISING COMMITTEE:

Supervisor:

Gary Kocurek

David Mohrig

Gregory Frébourg

Dune Behavior in a Multidirectional Wind Regime: White Sands Dune Field, New Mexico

by

Anine Oehlenschlaeger Pedersen, B.Sc.

Thesis

Presented to the Faculty of the Graduate School of

The University of Texas at Austin

in Partial Fulfillment

of the Requirements

for the Degree of

Master of Science in Geological Sciences

The University of Texas at Austin

August 2014

Acknowledgments

This research was supported by grants from the National Science Foundation EAR-0921659 and Shell Exploration and Production Company. I am grateful to Hildy Reiser and David Bustos, White Sands National Monument, for facilitating this study. Finally, a personal thank you to Jarl, Elise, and Esben Pedersen, and Colin McNeece for their tireless love and support.

Abstract

Dune Behavior in a Multidirectional Wind Regime: White Sands Dune Field, New Mexico

Anine Oehlenschaeger Pedersen, M.S.Geo.Sci.

The University of Texas at Austin, 2014

Supervisor: Gary Kocurek

As with most dune fields, the White Sands Dune Field in New Mexico forms in a wind regime that is not unimodal. In this study, dune behavior at White Sands was documented from a time series of five lidar-derived digital elevation models (DEM) and compared to a record of wind direction and speed during the same period. For the study period of June 2007 - June 2010, 244 sand-transporting wind events occurred and define a dominant wind mode from the SW and lesser modes from the NNW and SSE. Based upon difference maps and tracing of dune brinklines, overall dune behavior consists of migration to the NE, but with along-crest migration of dune sinuosity to the SE. Permutations of the DEMs allow matching specific dune behavior with wind modes. The SW winds are transverse to dune orientations and cause most forward migration. The NNW winds cause along-crest migration of dune sinuosity and low stoss bedforms, as well as SE migration of NE-trending dune terminations. The SSE winds cause ephemeral dune deformation, especially crestal slipface reversals. Dune deformation occurs because

of unequal deposition along the lee face as a function of the incidence angle formed between the wind and the local brinkline orientation. Incidence-angle control on dune deformation and types of lee-face surface processes allows for an idealized model for White Sands dunes. The dunes behave as complex systems in which each wind event deforms the dune shape, this new shape then serves as the configuration for the next wind event.

Table of Contents

List of Figures ix

1. Introduction 1

2. Study Area 3

3. Methods 6

4. Results and Discussion 12

    4.1 Wind Characterization 12

    4.2 Dune Behavior 25

    4.3 White Sands Dune Model 38

        4.3.1 Model Basis 38

        4.3.2 Model 42

    4.4 Predicting Dune Migration and Deformation 43

5. Conclusions 45

Bibliography 48

List of Figures

Figure 1: Location map 4

Figure 2: June 2007 digital elevation model with traced brinklines 7

Figure 3: Example difference map and migration calculation 9

Figure 4: Total wind rose 13

Figure 5: Wind roses by month 15-16

Figure 6: Frequency plot of wind-event duration 19

Figure 7: Monthly frequency plots of shear stress and wind-event duration by wind regime mode 21-22

Figure 8: Total potential sediment flux by direction 24

Figure 9: General dune behavior between June 2007-June 2010 26

Figure 10: Plot of sinuosity vs. along-crest:crest-normal migration 28

Figure 11: Dune behavior in response to prevailing SW winds 30

Figure 12: Dune behavior in response to subordinate NNW winds 32

Figure 13: Dune behavior in response to subordinate SSE winds 34

Figure 14: Aerial image of local crestal reversed slipfaces 36

Figure 15: Aerial image showing exposed strata and tracing of crest-normal and along-crest migration 37

Figure 16: Model for sinuous dune migration, deformation and surface processes based upon incidence angles for the resultant for the three wind modes 43

Figure 17: Plot of local incidence angles vs. 2007-2010 migration distance 46

1. Introduction

Most aeolian dunes form in a wind regime that is not unimodal. Over the long-term where the overall wind regime is not changing, dunes assume an orientation that is as perpendicular as possible to all components of the total wind regime, the gross bedform-normal orientation of Rubin and Hunter (1987). Observations of individual dunes over time or plan-views of dune cross-strata in the rock record, however, show that dunes commonly change shape as they migrate (i.e., deform) or show large-scale deformation such as along-crest migration of dune sinuosity (e.g., Rubin, 1987; Rachal and Dugas, 2009; Ewing and Kocurek, 2010a). Changes in dune shape or in dune-field pattern can arise because of changes in boundary conditions over time (Kocurek and Ewing, 2005; Ewing and Kocurek, 2010b). However, even under steady state conditions dunes and dune-field patterns exist in a state of dynamic equilibrium, in which statistical parameters of the dunes remain constant, but the dunes themselves deform as they migrate so that it is commonly difficult to identify individual dunes in aerial photos separated by years. Many changes in dune shape result from dune-dune interactions, in which dunes collide and reform (e.g., Elbelrhiti et al., 2005; Hersen and Douady, 2005; Ewing and Kocurek, 2010a; Kocurek et al., 2010; Génois et al., 2013). Less addressed are changes in dune shape where dune interactions are not occurring.

The purpose of this work is to explore dune deformation with migration in a non-unimodal wind regime through a time-series of airborne lidar-derived digital elevation models (DEM). Linking of dune migration and deformation evident in the DEMs with the

recorded winds during the same period allows for the identification of specific modes of dune migration and deformation with components of the wind regime. Eastwood et al. (2012) demonstrated that dunes deform incrementally with each sand-transporting wind event because deposition and erosion are not uniform across the lee face. This study addresses the larger time scale of dune deformation as specific to characteristic modes of the wind regime as repeated over months and years. Can dune migration and deformation be predicted from the net resultant of the wind? Conversely, does each wind event incrementally redefine dune shape such that the next wind event builds from new antecedent conditions, and long-term dune-shape change cannot be predicted beyond gross orientation of the dune? The latter behavior would identify aeolian dunes as complex systems with an attractor defined by the dune orientation and general dune type, but preclude a prediction of exact shapes over time (c.f., Werner, 1995; 1999).

2. Study Area

White Sands Dune Field is located in south-central New Mexico, situated within the Tularosa Basin between the San Andres Mountains and the Sacramento Mountains (Fig. 1). The entire dune field covers an area of roughly 500 km^2, and is bounded to the west by a deflationary gypsum plain, Alkali Flat, and active playas occur farther to the west in the lowest part of the basin. The southern portion of the dune field is encompassed within the White Sands National Monument. The dune field originated ~ 7 ka with the onset of regional aridity and a step-wise retreat of Pleistocene Lake Otero, in which the dunes were sourced through deflation of exposed gypsum lake beds (Langford, 2003; Kocurek et al., 2007; Baitis et al., 2014).

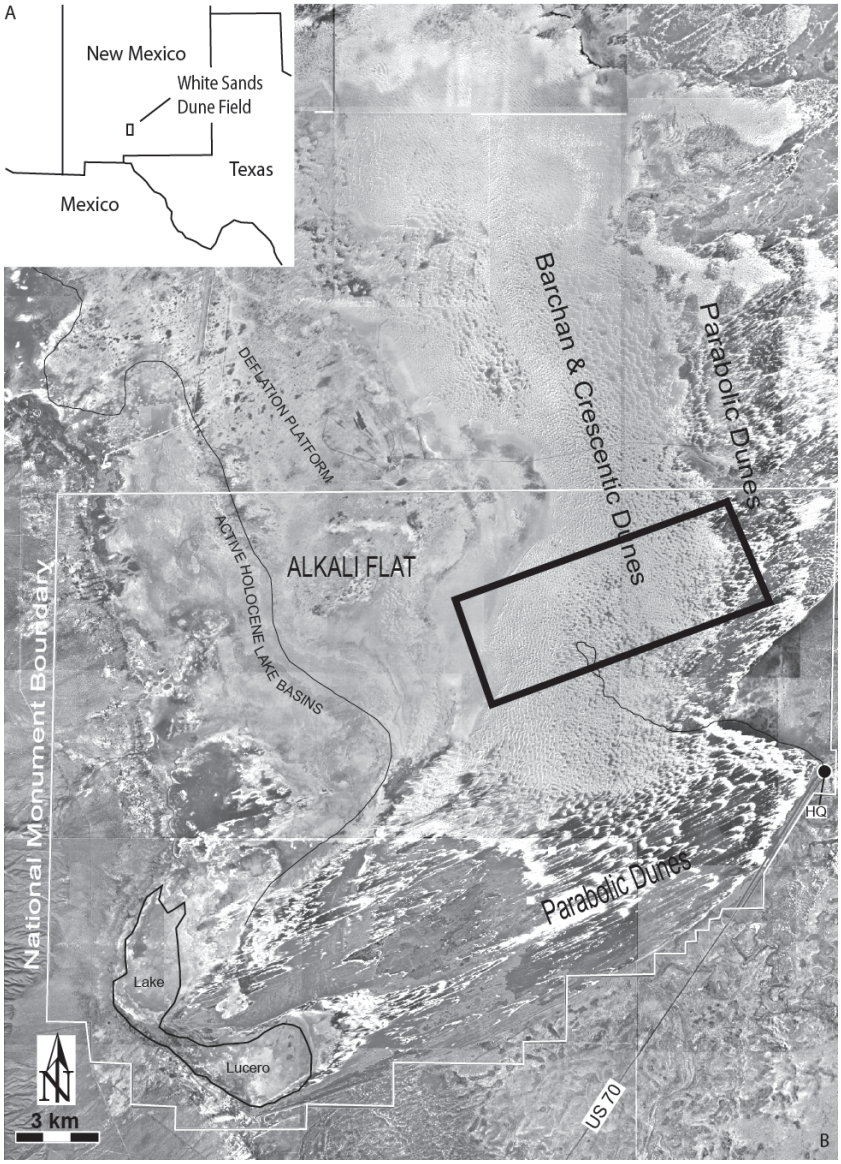

Figure 1: White Sands Dune Field in south-central New Mexico. The dune field consists largely of crescentic and barchans dunes, but crescentic dunes are transitional to parabolic dunes that occur along the eastern and southern periphery. Note Alkali Flat SW of the dune field and active playa Lake Lucero. Outline of national park shown with park headquarters (HQ). Rectangle indicates lidar survey area used for this study.

The core of the dune field consists of crescentic and barchans dunes, with a rim of parabolic dunes to the north, east and south (Fig. 1). In a field-scale study based upon a

digital aerial photo taken in 2003, Ewing et al. (2006) gave dune crestline orientation as 345°, average crestline length as 247 m, and average dune spacing as 136 m. The net wind resultant is toward 065° and based upon a decadal wind record at Holloman AFB, located ~ 10 km east of the dune field (Jerolmack et al., 2011). This study is based upon a time-series of airborne lidar surveys over a representative portion of the dune field populated by barchan and crescentic dunes (Fig. 1). Detailed analysis of dune parameters within the area of the lidar surveys is given in Baitis et al. (2014). The White Sands Dune Field has been the subject of many studies, including McKee (1966), Fryberger (2003), Langford et al. (2009), Rachal and Dugas (2009), and Jerolmack et al. (2011, 2012).

3. Methods

Airborne lidar topographic surveys were conducted over the 38.8 km^2 (15 mi^2) area of the White Sands Dune Field on 9 June 2007, 7 June 2008, 24 January 2009, 8 September 2009 and 5 June 2010 (Fig. 1). The staggered nature of the surveys was intended to capture dune morphological changes that occur with seasonal variations in the wind regime. The lidar surveys in June 2007 and June 2008 were flown by the Center for Space Research at the University of Texas at Austin, using an Optech ALTM 1225 lidar instrument integrated with an Ashtech Z-12 dual frequency GPS receiver and a Litton LN-200 inertial measurement unit aboard a Cessna 206 Turbo Stationair. Laser pulse rate frequency was 100 KHz, yeilding approximately 5 points per square meter of Earth's surface, and over 16 million points within the survey area. The data is at 1 m/pixel spatial resolution with ~ 0.1 m vertical resolution. The remaining surveys were flown by the National Center for Airborne Laser Mapping (NCALM) using a laser pulse rate frequency of 125 kHz, which results in 5-6 XYZ points per square meter, yielding approximately 20 million points. Lidar data were processed to yield digital elevation models (DEM), and the airborne GPS (ground positioning system) was geo-referenced to stations at the Alamogordo Regional Airport and Space Harbor on the White Sands Missile Range. Additional geo-referencing of all DEMs was done using Geographic Information Systems software (ArcGIS) and 135 stationary objects within the survey area.

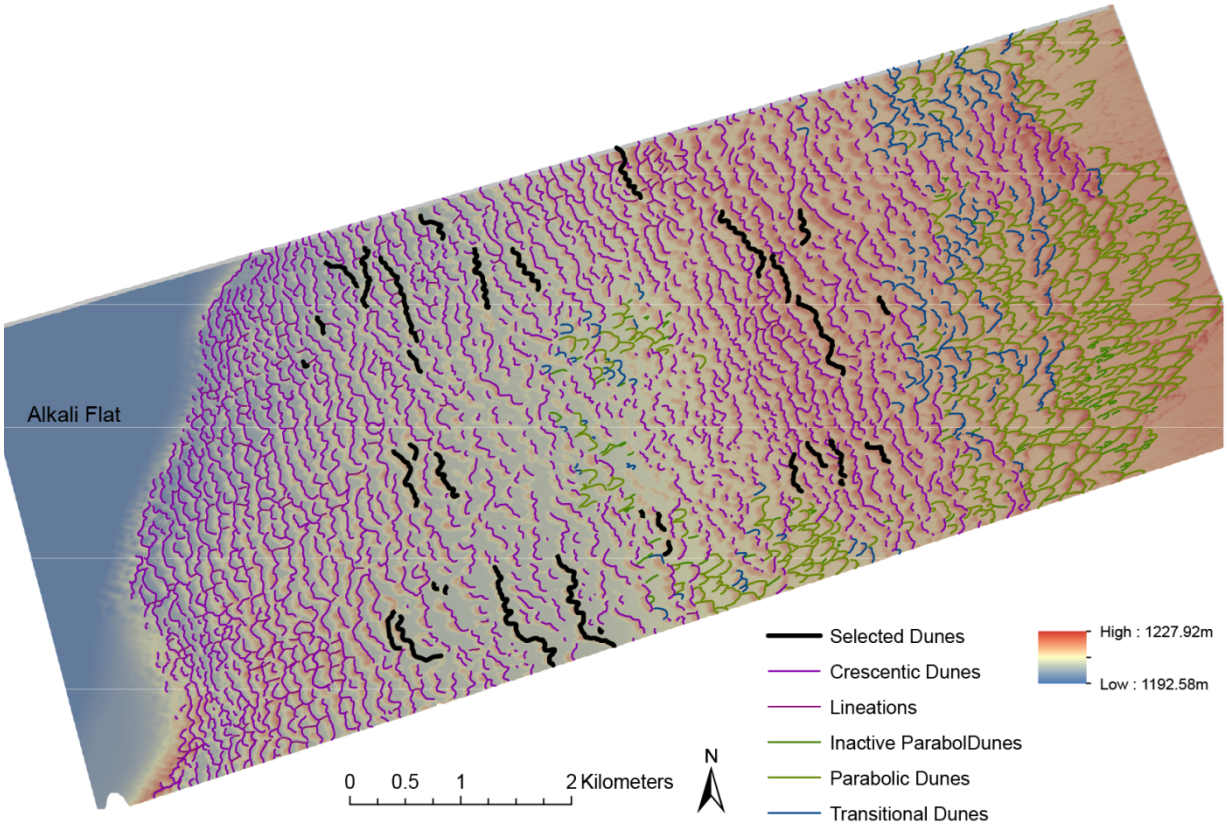

Figure 2. June 2007 DEM derived from lidar survey (Fig. 1). Elevation scale shown by color bar. Dune brinklines were manually traced and are color-coded by dune type. Black brinklines indicated 24 dunes selected as representative of dune morphologies and selected for detailed analysis (Fig. 3).

The orientations of each individual dune brinkline for all DEMs were manually digitized using ArcGIS and following the methods of Ewing et al. (2006) (Fig. 2). Difference maps were created by subtracting an older DEM from a younger DEM in ArcGIS for all permutations of lidar surveys. These difference maps were then contoured to delineate the relative magnitudes of deposition and erosion that had occurred over the

time intervals. In addition to the lidar surveys, low-altitude aerial photos of the lidar area were taken in June 2008.

Twenty-four dunes were selected as representative of the dune morphologies within the survey area, and these were used for subsequent detailed analysis. Using a planform statistical tool in ArcGIS, each dune brinkline was segmented by points into straight-line dune segments, and migration distance was measured for each point for the time-series of DEMs (Fig. 3). Each brinkline segment also had a local orientation, which was used to determine local incidence angle (i.e., angle between the local brinkline and a primary wind vector). In addition, the permutations of DEMs and difference maps were searched overall for examples of dune behavior that correspond to specific wind directional modes.

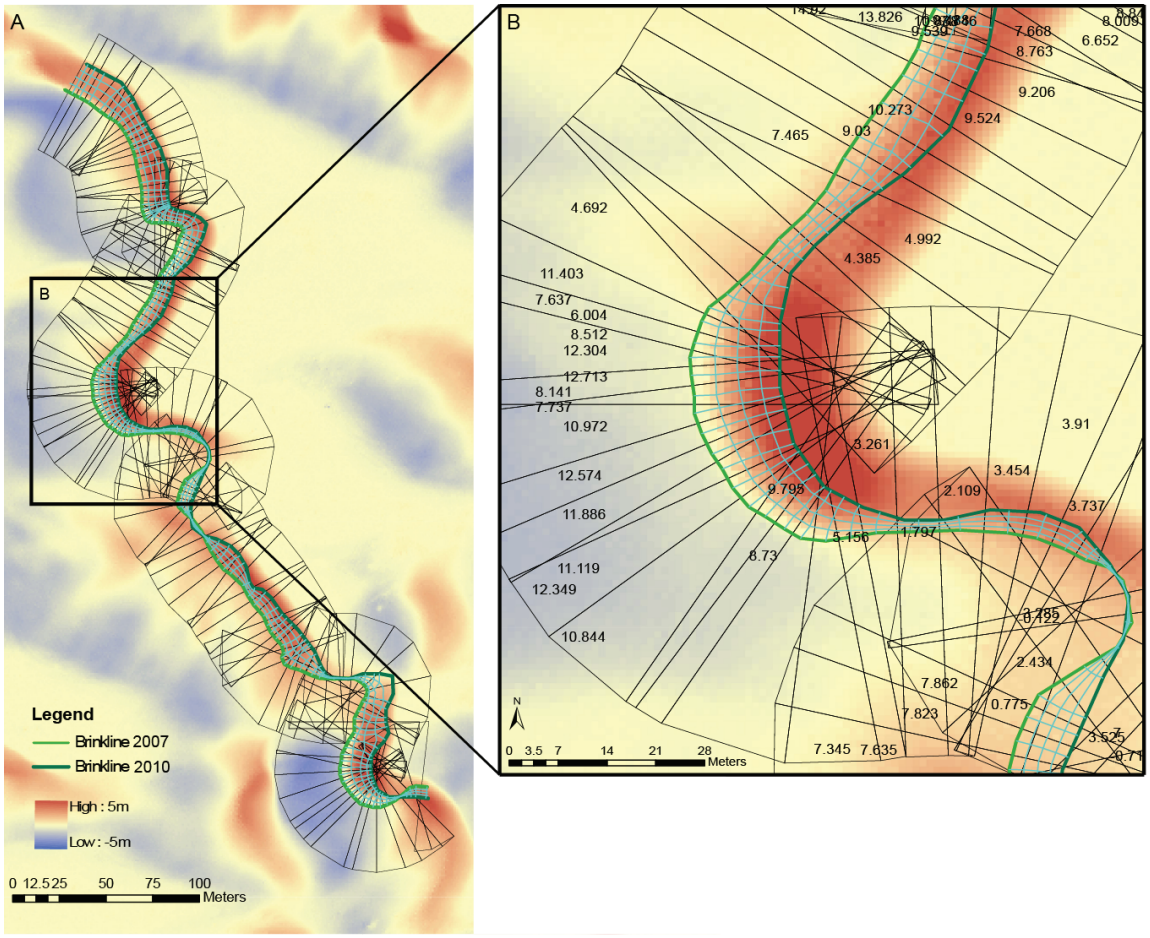

Figure 3. (A) Example of difference map created by subtracting the June 2007 DEM from the June 2010 DEM for one of the dunes selected for detailed analysis (Fig. 2). June 2007 and June 2010 brinklines shown with elevation differences indicating deposition (red) and erosion (blue). Dune brinkline was discretized by defining straight-line segments between points, and brinkline migration distance was calculated. (B) Enlargement of dune segment giving migration distances.

Wind data for the time interval between lidar surveys were collected at the NOAA National Climatic Data Center weather station at Holloman AFB, station #747320, and provided by MesoWest. Data consist of measurements of wind speed and direction, with

resolutions of 1 mph and ~10°, respectively, and measurements were taken at a height z = 10m above the surface. The intervals at which the wind measurements were taken were inconsistent, ranging from every few minutes to every hour (most common). Therefore, when analyzing wind events from this data, all events ≤ 1 hr are binned together (i.e., the minimum wind event used is1 hr).

The critical shear velocity ($\boldsymbol{u_{*c}}$) for dune sand motion at White Sands was calculated as 0.3139 m/s based upon the equation of Shao and Lu (2000), which is derived from data of Iverson and White (1982) for a range of grain sizes that includes most aeolian sand:

$$u_{*c} = \sqrt{0.0123\left(sgd + \frac{3\times10^{-4}\,kg/s^2}{\rho_f d}\right)} \quad (1)$$

where $s = \rho_s/\rho_f$ where ρ_s is the sediment density (taken as 2320 kg/m^3 for gypsum), ρ_f is the fluid density, g is the acceleration due to gravity, and d is nominal grain diameter (taken as 0.4 mm). Wind speeds measured at Holloman AFB were converted into $\boldsymbol{u_*}$ using the law of the wall:

$$\boldsymbol{u_z} = \frac{\boldsymbol{u_*}}{\boldsymbol{k}}\,\mathbf{ln}\left(\frac{\boldsymbol{z}}{\boldsymbol{z_0}}\right) \quad (2)$$

where u_z is the wind speed at height z = 10 m, κ is von Kármán's constant (0.407) and z_0 = 0.2 mm is the surface roughness based upon dune sand at White Sands (Eastwood et al., 2012). The calculated wind speed, as measured at Holloman AFB, for $\boldsymbol{u_{*c}}$ is 8.34 m/s, and all wind measurements below this value were excluded. For each sand-transporting wind (i.e., ≥ $\boldsymbol{u_{*c}}$), potential sediment flux,$\boldsymbol{Q_s}$, was calculated using the White (1979)

formulation of the Kawamura (1951) equation, as corrected by Namikas and Sherman (1997),

$$\boldsymbol{Q_S = 2.61\ \frac{\rho_f u_*^3}{g}\left(1 - \frac{u_{*c}}{u_*}\right)\left(1 + \frac{u_{*c}}{u_*}\right)^2}. \quad (3)$$

Wind roses were generated using WindRose Pro, which creates a joint frequency plot of wind direction and speed, for the periods between lidar surveys, for each month between June 2007 and June 2010, and for the entire 3 yr period.

Observed differences in traced brinkline shape, and depositional/erosional patterns from the difference maps were compared to the wind regime for that period in order to identify changes in dune morphology as a response to components of the wind regime. Measured migration rates for dune segments of the 24 dunes selected for detailed analysis were plotted to determine controls on dune segment migration and dune deformation.

4. Results and Discussion

4.1. Wind Characterization

Figure 4 shows a rose diagram for all winds at or above threshold speed as recorded at Holloman AFB between 9 June 2007 and 5 June 2010. The plot compiles wind frequency for 10º segments of the compass, with each segment binned by wind speed. Three modes of the White Sands wind regime are apparent: (1) dominant SW winds with a resultant toward 064º, which accounts for 53% of the winds, (2) NNW winds with a resultant toward 165º, which accounts for 26% of the winds, and (3) SSE winds with a resultant toward 345º, which accounts for 21% of the winds.

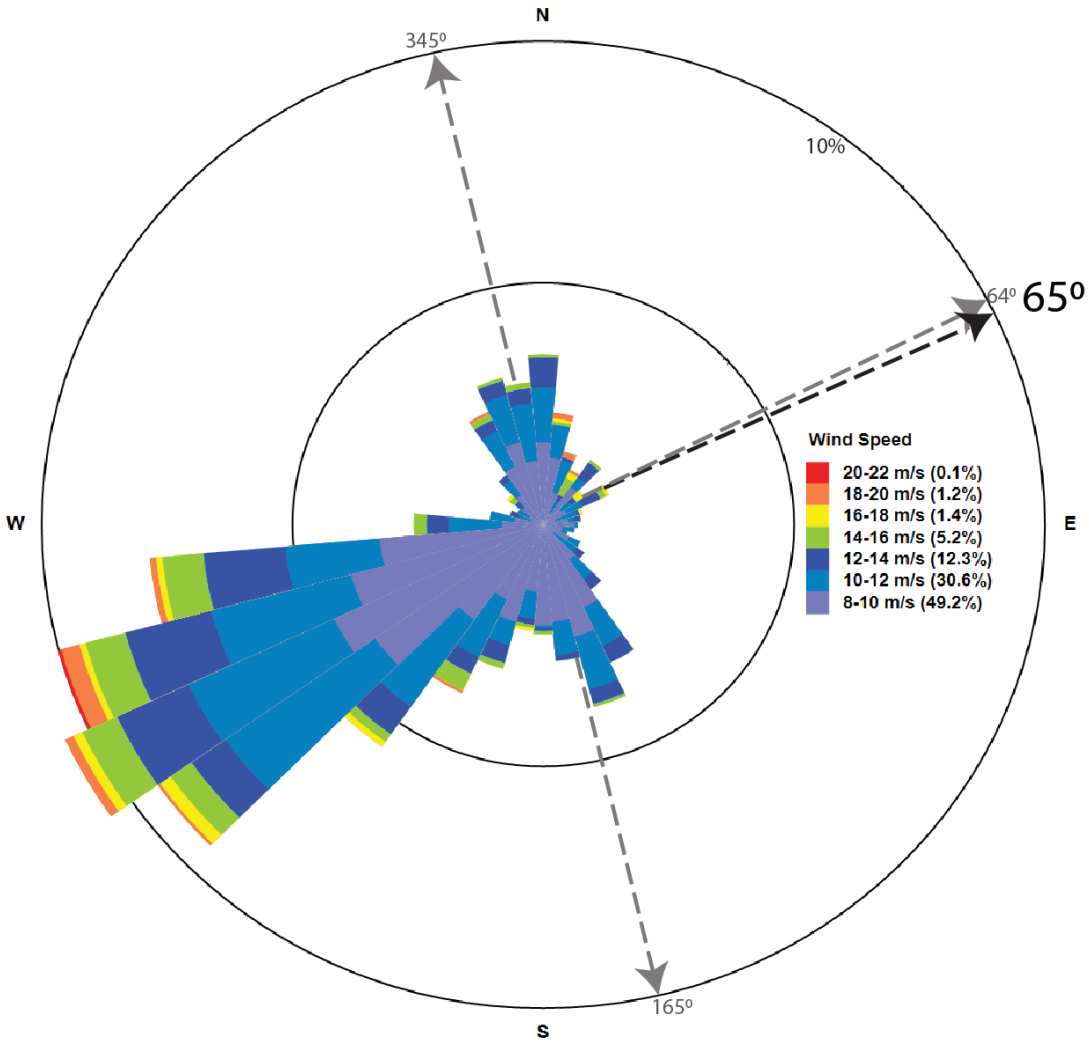

Figure 4. Wind rose for all winds at or above threshold speed between 9 June 2007 and 5 June 2010 as recorded at Holloman AFB. Winds are plotted by 10° compass segments with segment length based upon frequency. Segments are binned by wind speed. Note dominant mode of SW winds with a resultant toward 64°, and lesser NNW mode with a resultant toward 165° and SSE mode with a resultant toward 345°. Net resultant for all winds is toward 065°.

The rose diagram compares well to the rose diagram constructed from decades of wind measurements recorded at Holloman AFB (Fryberger, 2003). The total net resultant

toward 065° is also the same as that calculated by Jerolmack et al. (2011). The wind regime sampled during the total study period, therefore, appears representative of the long-term wind regime at White Sands. Note that the net resultant is nearly the same as the resultant for the dominant SSW winds, and that the resultants for the NNW and SSE winds are 180° apart. Nearly half of the winds are near threshold speeds, whereas winds above 16 m/s account for only 2.7% of the winds.

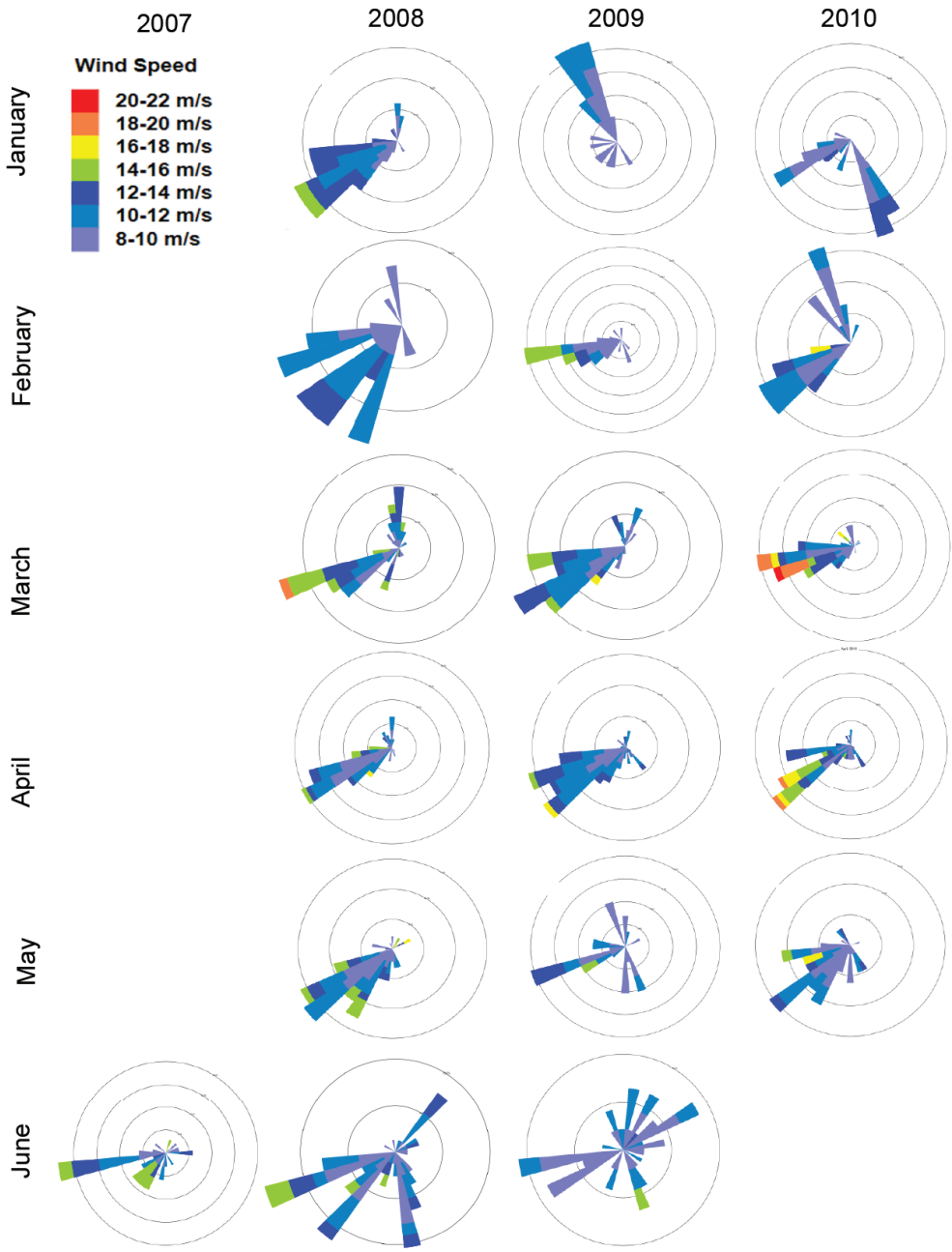

Figure 5. See caption on next page.

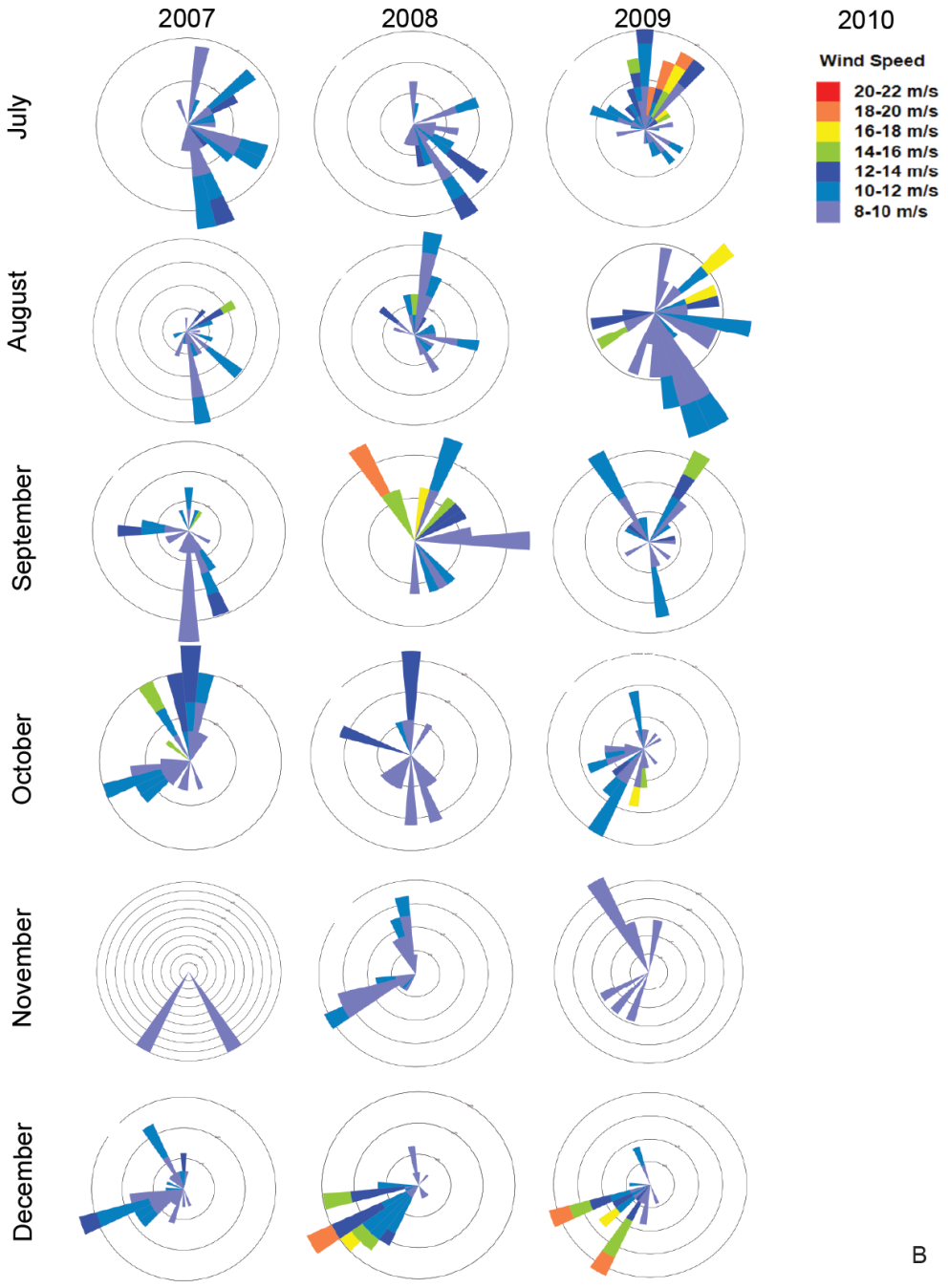

Figure 5. Total wind rose (Fig. 4) is broken into monthly wind roses for the study period. As with Fig. 4, winds are plotted by 10° compass segments with segment length showing wind frequency and binned by wind speed. Inner circles represent 5% steps of total data for that month, such that more circles occur with fewer measurements for the month. See text for discussion.

Figure 5 breaks the total wind rose (Fig. 4) into monthly roses in order to determine any seasonality in the wind regime. Previous work has reported that the dominant SW winds characterize the spring months, whereas the NNW winds occur largely with frontal passages in the fall, winter and early spring, and the SSE winds occur during the summer with monsoonal flow (McKee, 1966; Fryberger, 2003; Kocurek et al., 2007). If the total study period is indeed representative of the long-term wind regime, then the seasonal characterization is over-simplified. With the exception of the spring months of March – May when SW winds almost exclusively dominated, most months showed marked differences in wind speed and direction from year to year. While the SW winds during March – May accounted for 60% of all SW winds, SW winds also dominated in December – February overall, and were generally insignificant only in July – September. SSE winds did occur most frequently during the summer months of June – September, but also occurred in January and October. The NNW mode did occur in the fall and winter months of October – February, but 42% of the NNW winds occurred in June – August. These summer NNW winds were frequently recorded along with precipitation and these winds likely represent storm-associated winds developed during the monsoon season. The months of January and June – October had the greatest variability in wind directions. November was the least windy month. Overall, based upon the total study period, the wind regime at White Sands is characterized by: (1) the emergence of the dominant SW winds in December, which continue through May but with periods of lesser NNW and SSE winds, and (2) highly variable winds with winds from all three modes during June – November. Although the total three-year study period

is representative of the long-term wind regime as reflected by the resultant, a year-by-year calculation of the resultant shows that the resultant varies annually. The resultant for June 2007 – May 2008 is 60.6°, June 2008 – May 2009 is 68.4°, and June 2009 – May 2010 is 68.5°.

Characterization of the wind regime during the study period by wind frequency shows that there were ~ 1.5 times as many calm days as days with at least one wind measurement at or above threshold speed (666 vs 427 days). For the 427 wind days, there were ~ 1600 recorded wind speeds at or above threshold speed. These measurements were grouped into "wind events", defined as one or more recorded wind speeds at or above threshold speed and separated by at least 12 hr of winds below threshold speed from other winds events. Using this definition, 358 wind events were identified, but 114 of these were single measurements, which possibly represent winds of such short duration as to have little or no sand-transporting potential. The remaining 244 wind events represent ~ 81 events per year. Including the "single reading wind events" (for which a 1 hr duration was assigned, see Section 3), the average duration of a wind event was 4.7 hr, and the longest event lasted 53 hr (Fig. 6). Wind events of a few hours were clearly the most frequent, and wind events lasting longer than 10 hours accounted for only 11% of the total. The average wind speed of all wind events was 10 m/s, but these ranged from just above threshold velocity to 15.4 m/s, with a highest recorded gust being 16.4 m/s.

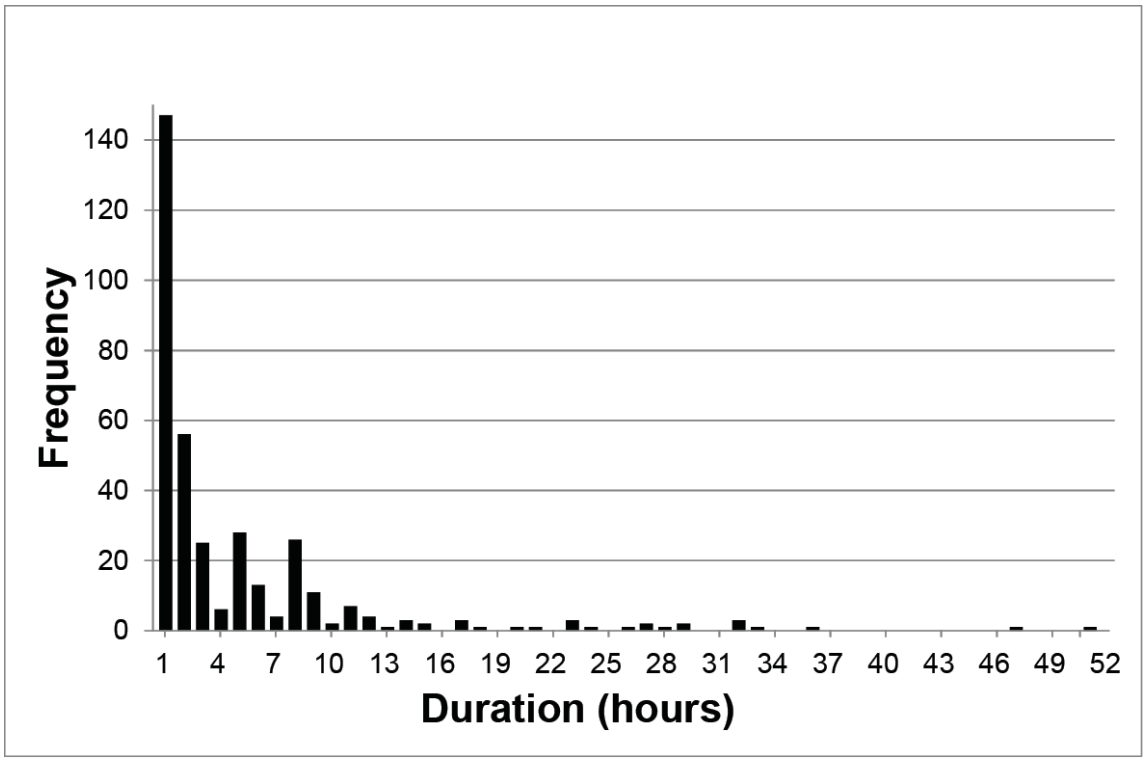

Figure 6. Frequency plot of wind-event duration by hours. The large number of 1 hr events includes 114 single entries of winds at or above threshold speed, which may represent insignificant sand transport. Note overall decrease in event duration, with events greater than 10 hr being uncommon. The average wind event was 4.7 hr in duration, the longest was 53 hour.

Because the sand-transport capacity of a wind event is a function of the magnitude of u_* and the duration of the event, all winds at or above threshold speed were converted to u_* (see Section 3) and plotted with wind-event duration by month and grouped into SW, SSE and NNW modes (Fig. 7). The SW winds emerged in December, extended through February as the dominant sand-transporting wind, and then greatly increased in both u_* and event duration in March – May, with a peak in April. These spring winds clearly represent the primary sand-transporting events. Incursions by the

NNW winds during this period were of significantly lower u_* and generally represented by short duration events, whereas the SSE winds were a yet lesser background component. Clear diminishing of the SW winds in both u_* and event duration occurred by June, the SSE winds emerged as frequent short-term events, as did the NNW winds to a lesser extent. The summer July – August wind pattern, diminishing in September, showed insignificant SW winds, and dominance by moderate energy SSE and NNW winds largely in high frequency, low duration events. An overall diminished wind regime characterized October – November, especially with the loss of SSE winds by November.

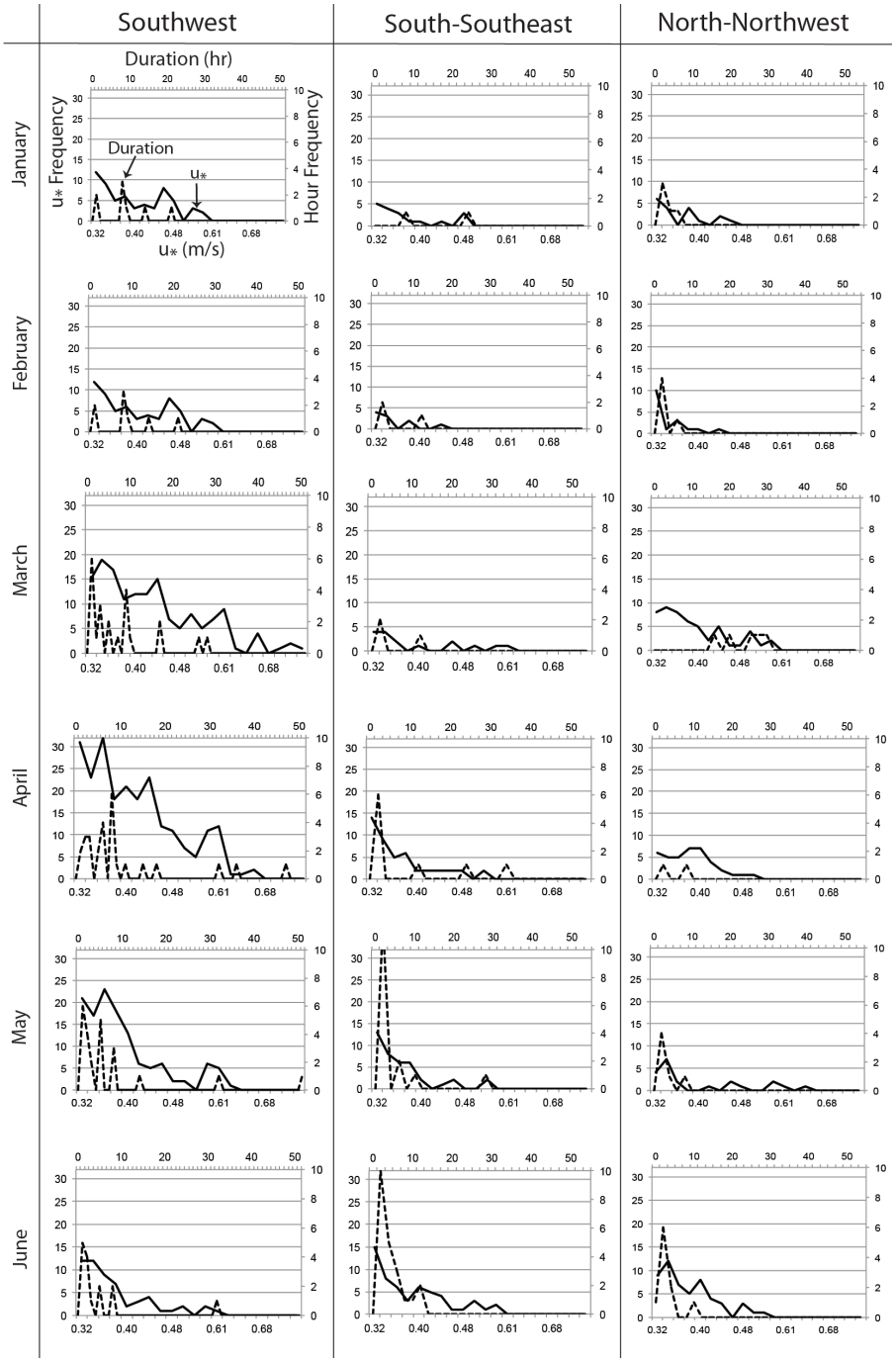

Figure 7. See caption on next page.

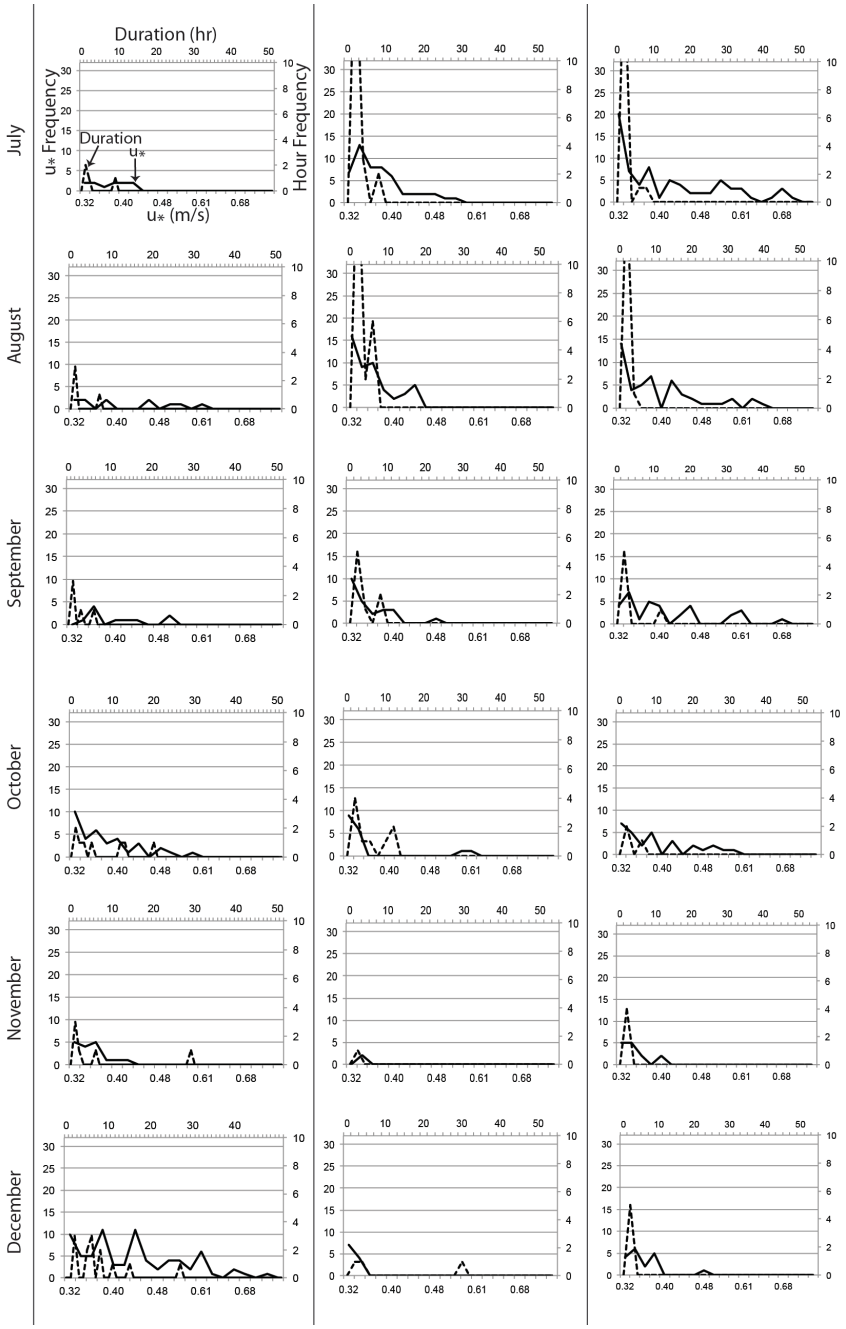

Figure 7. Plot of u_* (solid line) and wind-event duration (dashed line) by month for SW, SSE and NNW modes of the total wind regime during the study period. The y-axis plots frequency (u_*on the left, duration on the right), the bottom x-axis is u_* (m/s) and the top x-axis is duration of wind events in hours. See text for discussion.

Based upon the concept of geomorphic work from Woman and Miller (1960), Jerolmack and Brzinski (2010) found that the most constructive wind at White Sands based upon the combination of magnitude and frequency has a $u_* = 0.39$ m/s. For the study period, the average u_* for all events was 0.37 m/s, but the most frequently occuring magnitude of any component of the wind regime was 0.39 m/s. Moreover, this value of u_* most frequently occurred with the SW winds. In terms of both the most constructive wind and the occurrence of high values of u_* in wind events of long duration, the SW winds clearly dominant over the SSE and NNW winds.

Calculation of the potential sand flux $\boldsymbol{Q_s}$ (see Section 3) and plotting by frequency within compass segments yields a reformulated sand rose in which sand transport by the three modes of the wind regime is given (Fig. 8). Aspects such as sand moisture and other factors that may inhibit sand transport are unknown and ignored here. In contrast to the simple wind rose (Fig. 4), the overwhelming dominance of sand transport by the SW winds is evident. Moreover, although the opposing NNW and SSE appear roughly sub-equal in the wind rose (Fig. 4), the NNW winds clearly are a greater sand-transporting wind than the SSE winds.

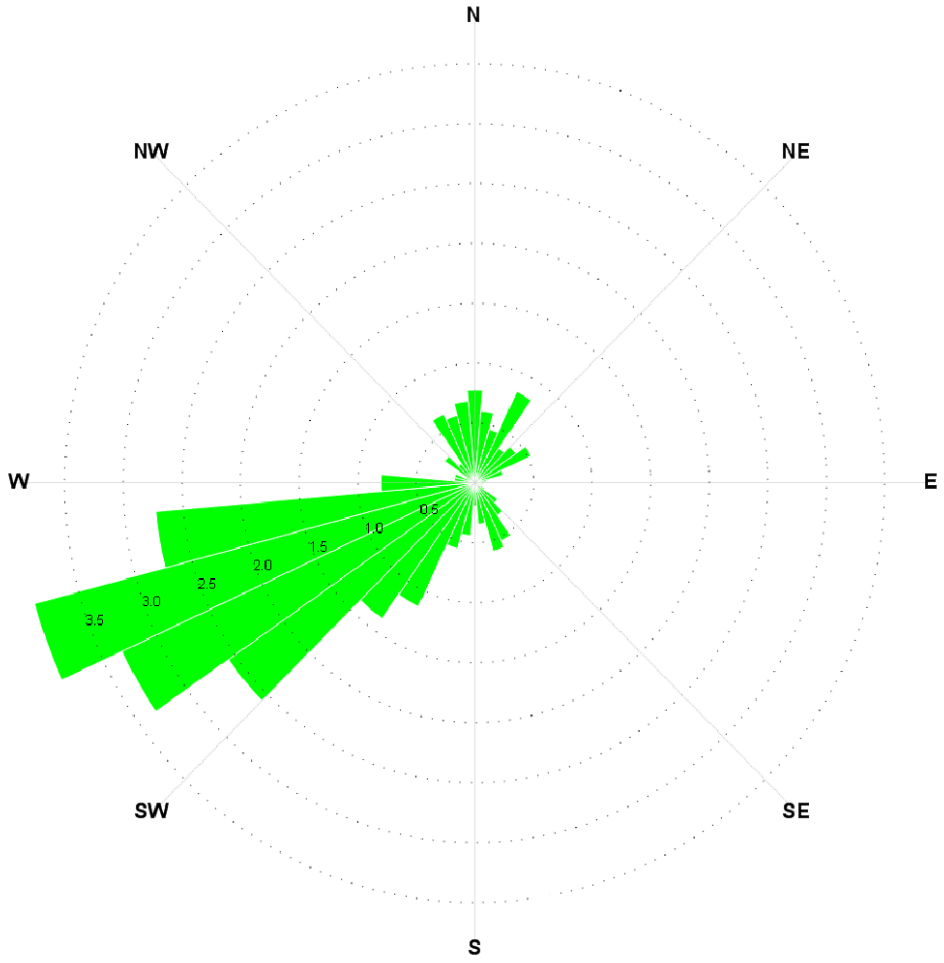

Figure 8.Total potential sediment flux $\boldsymbol{Q_s}$ for the study period shown as a rose diagram. The dominance of sand transport by the SSW is more apparent than in the wind rose diagram (Fig. 4), and the sand-transporting capacity of the NNW winds is significantly greater than that of the SSE winds.

4.2. DUNE BEHAVIOR

As evident from Section 4.1, the dunes at White Sands form within a tri-modal wind regime with a dominant wind from the SW, and lesser modes from the NNW and SSE. Except for the smallest barchans, dune size precludes dune reformation with each wind event (i.e., the dune reconstitution time >> wind cycle duration). Previous work (Ewing et al., 2006; Kocurek et al, 2007) demonstrated that the average dune crestal trend of 345° is borderline transverse to the net wind resultant of 065° in the classification of Hunter et al. (1983). Given that the resultant from the SW winds is nearly the same as the net resultant, the 10° departure of the average crestline trend from being perfectly transverse results from the effects of the NNW and/or SSE winds (Jerolmack et al., 2011). Whereas the difference map created by subtracting the June 2007 DEM from the June 2010 DEM shows overall dune behavior over the three-year study period, other difference maps constructed from the time-series of DEMs allow for characterization of dune deformation in response to the three winds modes, albeit that no time period between lidar surveys was exclusively dominated by a single wind mode.

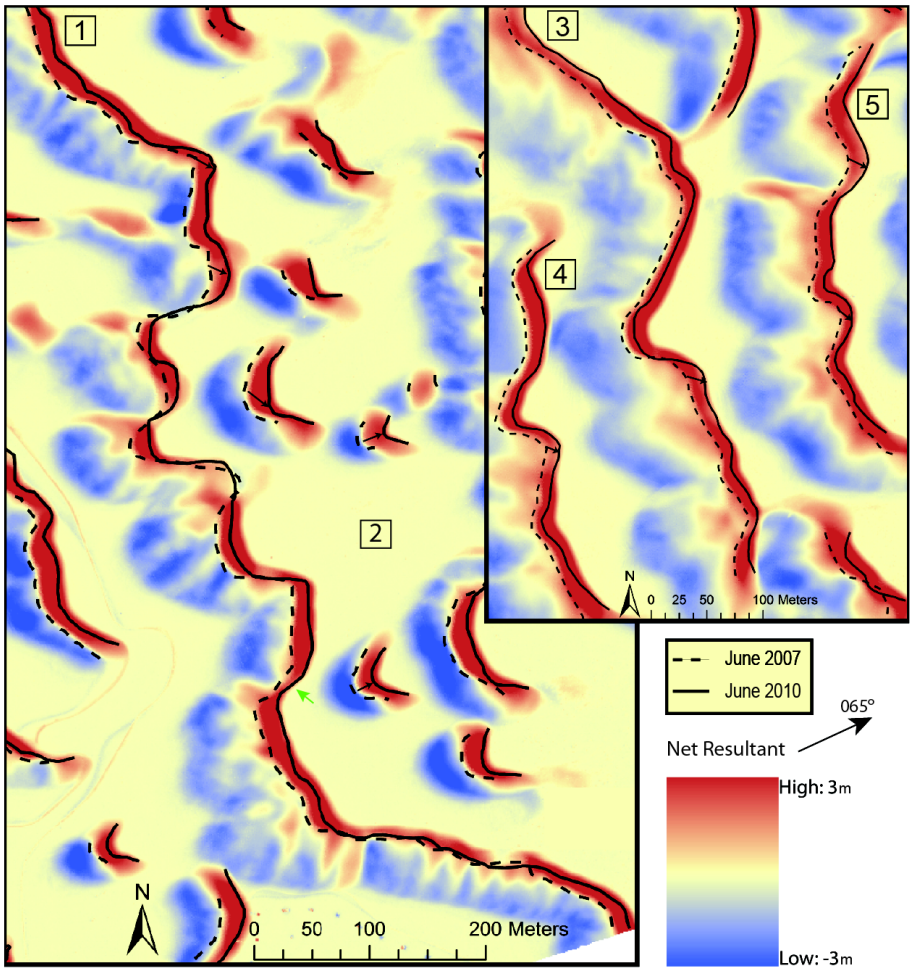

Figure 9. Difference map constructed by subtracting the June 2007 DEM from the June 2010 DEM, with brinklines shown. Color scale reflects erosion (blue) and deposition (red) at a fixed point. Area 2 shows a cluster of barchan dunes in which small dunes migrated parallel to the resultant, whereas larger barchans migrated forward and crabbed to the SE, as indicated by arrows. Fairly uniform forward migration occurred for lower sinuosity dunes (dunes 3 – 5) except along segments of high sinuosity at convex-downwind noses (dune 3), which also migrated along-crest to the SE (as indicated by arrow). Very long and sinuous dune 1 shows non-uniform brinkline migration, resulting in dune deformation. Convex noses migrated along-crest (arrow) and extended such that 2007 and 2010 brinklines largely coincide along the flanks of the noses, except along some SE flanks (green arrow) where deposition reflects along-crest migration of the nose. Pattern of erosion and deposition on the stoss slope which are oriented normal to the crestline reflects along-crest migration to the SE of low superimposed dunes.

Figure 9 shows difference maps of dunes representative of the entire study period (June 2007 DEM subtracted from June 2010 DEM), with the 2007 and 2010 brinklines traced. The net resultant for this period was 065°. For the cluster of barchan dunes (area 2), the smallest dunes show simple migration to the NE (in the net resultant and SW wind resultant directions), whereas the larger dunes show a distinct lateral shift to the SE (indicated by arrows), which is generally referred to as "crabbing". The small barchan dunes may be sufficiently small to have reconstituted their shape to the SW winds that prevailed from February to June 2010 (see Fig. 5). The larger barchan dunes have a greater reconstitution time and their behavior reflects the overall wind regime. Dunes 3 – 5 represent typical crescentic dunes and these show fairly (but not entirely) uniform migration to the NE with stoss erosion and lee deposition, but the brinklines for convex-downwind segments show an along-crest migration (indicated by arrows) to the SE, similar to the crabbing evident in the larger barchans. On segments of high local sinuosity (center portion of dune 3), along-crest migration of the convex nose to the SE was sufficient such that the 2010 brinkline eroded through lee face deposits to intersect the 2007 brinkline. Dune 1 represents a very long crescentic dune with high sinuosity, in which significant dune deformation occurred. Convex-downwind noses both extended to the E and migrated along-crest to the SE (indicated by arrows). Along-crest migration of concave-downwind brinkline segments is less obvious, and is largely manifested in the along-slope migration to the SE of adjacent NW segments of the convex-downwind noses. As seen by the two brinklines, separated in time by three years, migration along the length of the crestline was far from uniform on this highly sinuous dune and the dune

has changed in shape (i.e., deformed). Dune 1 also shows a pattern of deposition and erosion on the stoss slope that is oriented roughly normal to the crestline. This pattern represents the migration of low amplitude bedforms superimposed upon the stoss slope, with a net along-crest migration to the SE (addressed below). Based upon discretization of the brinklines of 24 dunes (see Fig. 3), the average migration distance in the net resultant direction for the three year study period was 10.8 m (3.6 m/yr).

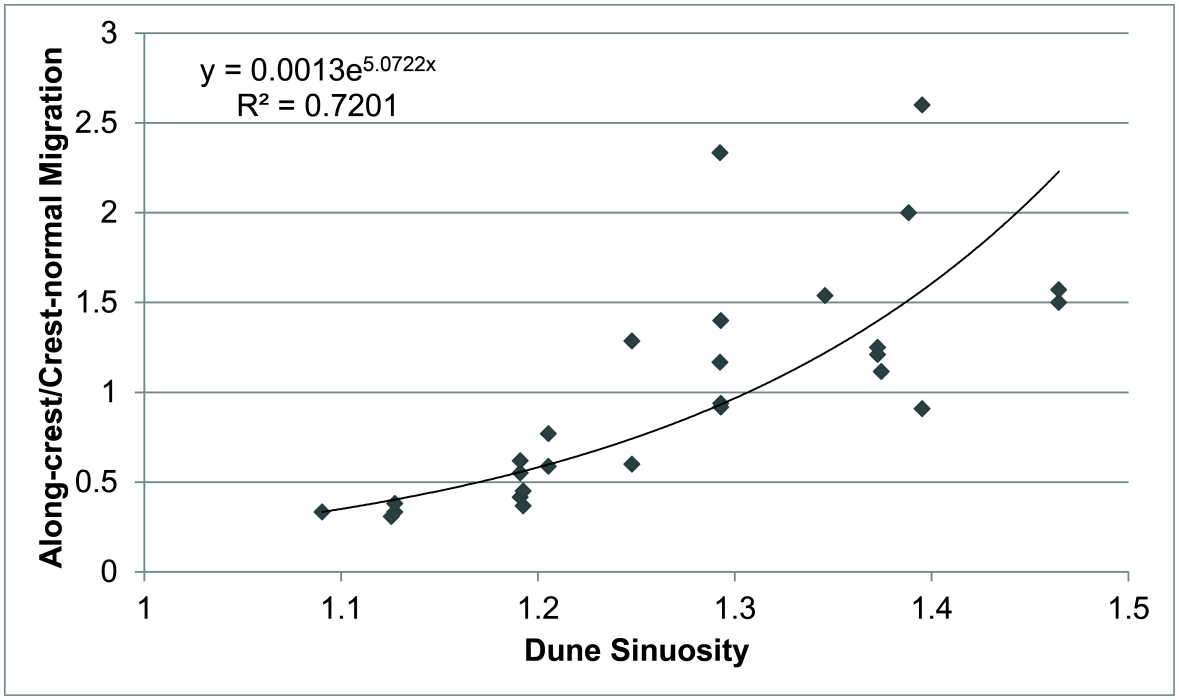

Figure 10. Plot of dune sinuosity (actual brinkline length divided by straight-line distance) against the ratio of along-crest over crest-normal migration for convex-downwind dune noses. The good correlation coefficient shows that along-crest migration increases with dune sinuosity.

The apparent correlation between dune sinuosity and along-crest migration of convex-downwind noses was tested by plotting the ratio of dune sinuosity against the ratio of along-crest over crest-normal dune migration (Fig. 10). For low sinuosity dunes, the ratio was as low as 0.3, but the ratio increased as dune sinuosity increased. For highly sinuous dunes, along-crest migration of convex-downwind noses was as great as 2.5 times that of crest-normal migration. This along-crest migration represents a large-scale deformation with dune migration and is explored below as a result of the tri-modal wind regime. The smaller scale of deformation, such as evident in Dune 1 (Fig. 9) and the slightly non-uniform migration of the brinklines in Dunes 3 – 5 (Fig. 9), is addressed below and in Section 4.3.

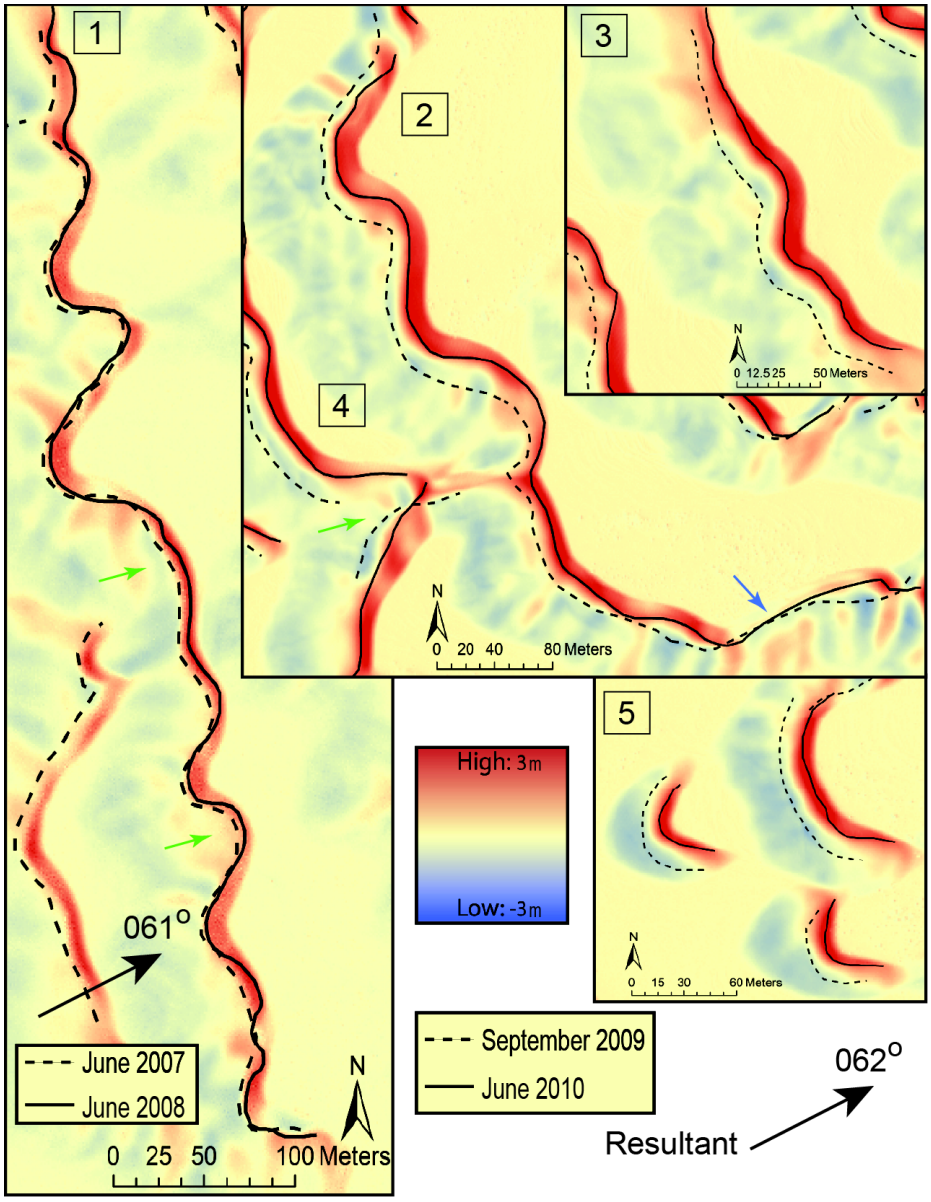

Figure 11. Difference maps constructed by subtracting the June 2007 DEM from the June 2008 DEM (dune 1), and the September 2009 DEM from the June 2010 DEM (dune 2 – 5). The resultant for the time interval reflects dominance by the SW winds in the spring months. Because the dunes are oriented nearly perpendicular to the dominant SW winds, greatest dune migration occurs towards the NE, but brinkline advance varies along dune width as a function of the incidence angle, especially evident on dune 2. Note coincidence of brinklines along flanks of convex noses whereas the center of the nose migrated forward (green arrows, dune 1).

Figure 11 illustrates the effects of the dominant SW winds by using a difference map constructed by subtracting the June 2007 DEM from the June 2008 DEM (dune 1), and a difference map constructed by subtracting the September 2009 DEM from the June 2010 DEM (dunes 2 – 5). Both time periods were dominated by SW winds in the spring months before the surveys (see Fig. 5), and the resultants were toward 061° (dune 1) and 062° (dunes 2 – 5). In comparison to the difference maps representing the NNW and SSE winds presented below, the SW winds clearly caused the greatest crest-normal migration of the dunes. Differences in brinkline advance, however, are apparent along the width of the dunes. Brinkline advance was greatest where the SW winds (as measured by the resultants) were transverse to the brinkline (centers of convex and concave segments of crescentic dunes; barchan dunes in area 5), and least where the resultant was at a very oblique angle or longitudinal to the brinkline (blue arrow, dune 2). For convex noses where the flanking brinklines of the nose were nearly parallel to the resultant, the noses extended to the NE but the successive brinklines coincide along the flanks of the nose (green arrows, dune 1). An extreme case of convex-nose extension is seen in dune 4 where brinkline definition has been lost and a ramp of depositional sand escaped from the dune and traveled up the stoss slope of the downwind dune (green arrow).

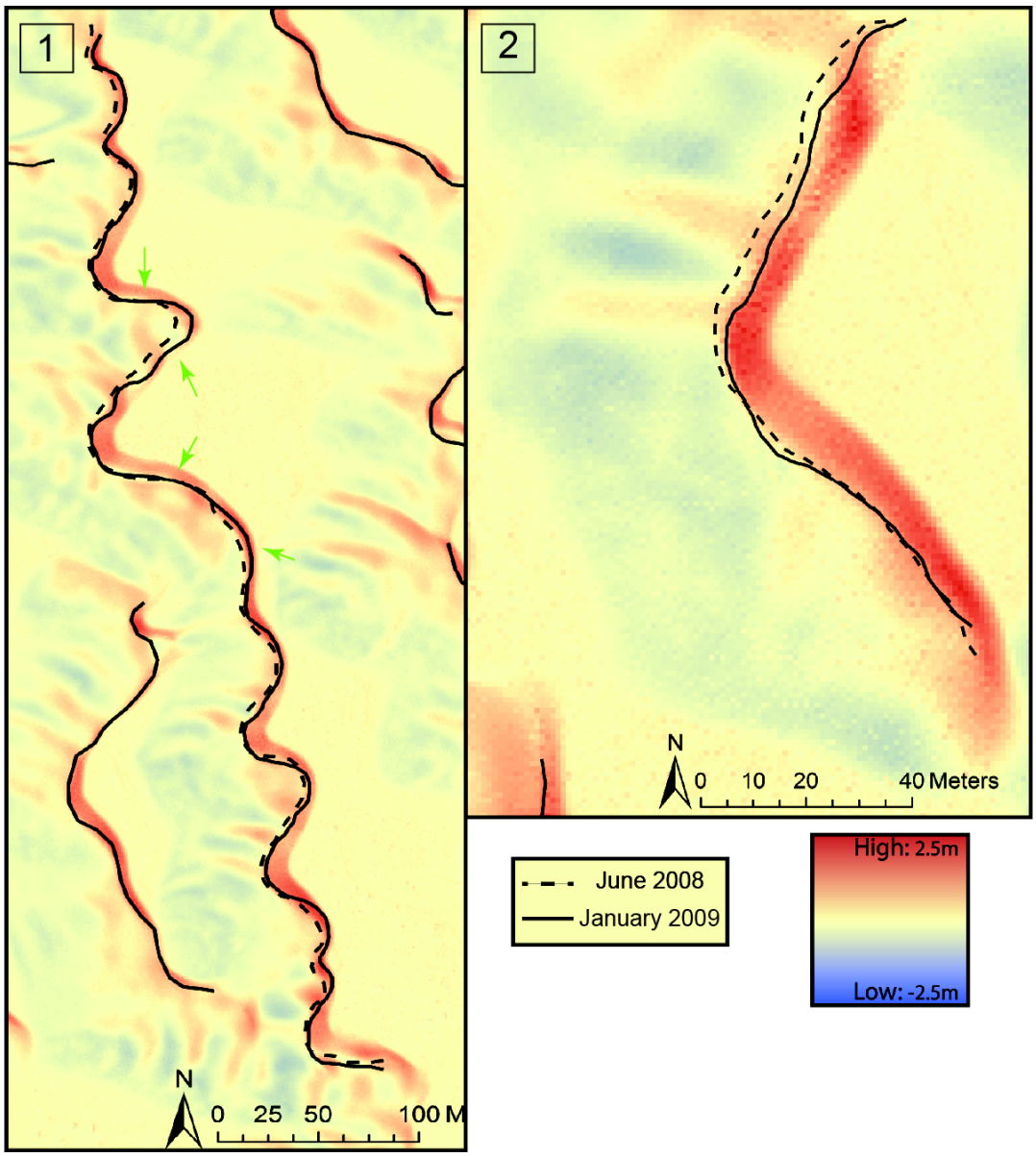

Figure 12. Difference map constructed by subtracting the June 2008 DEM from the January 2009 DEM, and showing the effects of the NNW wind mode. Along-crest migration of sinuosity (concave- and convex-downwind segments) is evident in which NNW and N winds were nearly transverse (green arrows, dune 1). NNE-trending dune termination (oblique incidence angle) migrated, whereas SSE-trending brinkline was nearly longitudinal to the primary winds and the brinklines coincide (dune 2). Stoss depositional/erosional pattern on dune 2 reflects migration of superimposed low bedforms under N and NNE winds.

Figure 12 shows dunes in difference maps constructed by subtracting the June 2008 DEM from the January 2009 DEM. Although a variety of winds occurred during this period, the NNW winds were well represented, especially during January, and the dunes show the effects of this wind mode. The along-crest migration of dune sinuosity evident in the three-year difference map (Fig. 9) can be confidently accredited to the impact of the NNW winds. Note that the June and January brinklines coincide along the NW flanks of the convex-downwind noses, whereas there was deposition and brinkline advance along the SE flanks (greens arrows on dune 1). Similarly, the NNE-trending dune termination of dune 2 (oriented at a high oblique angle to the NNW winds) advanced, but the SE-trending termination (oriented longitudinal to the NNW winds) did not. The erosion/deposition pattern on the stoss slope of dune 2 occurred with along-crest migration of the low superimposed dunes, most probably with winds from the N and NNE during this period.

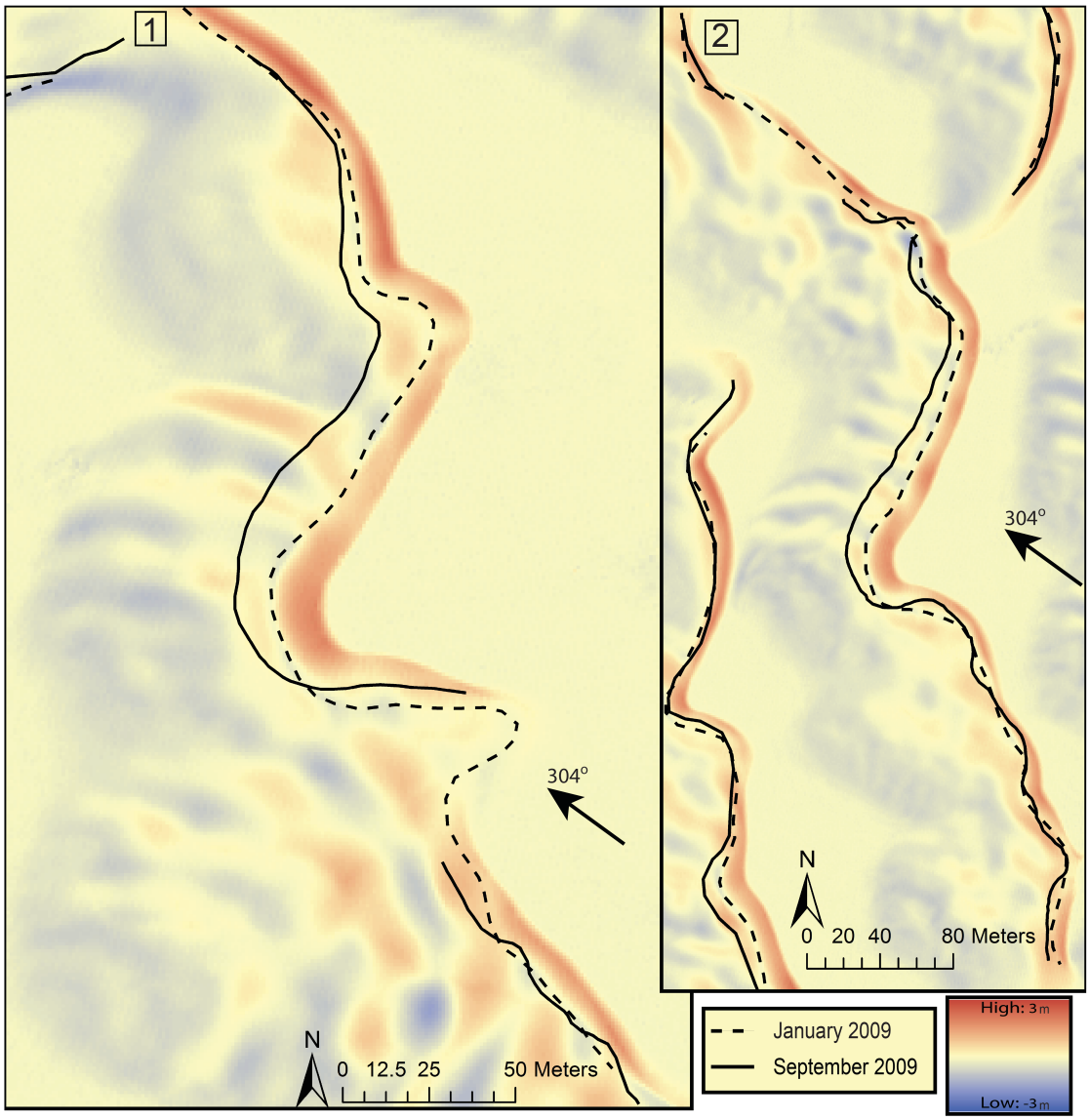

Figure 13. Difference map constructed by subtracting the January 2009 DEM from the September 2009 DEM, and showing the effects of the SSE wind mode. The wind resultant for the period was toward 304° and SSE winds prevailed in the August before the survey (Fig. 5). The primary features are the creation of Chinese walls or reversed crestal asymmetry where the September brinkline retrograded to the NW passed the January brinkline along transverse dune segments. Note that the difference map reflects the greater deposition/erosion pattern of the greater SW winds. Little change in brinklines is evident for brinkline segments oriented nearly longitudinal to the SSE winds (southern segments of dunes 1 – 2).

Figure 13 shows dunes in difference maps constructed by subtracting the January 2009 DEM from the September 2009 DEM and it captures dune behavior as a result of the SSE winds during August 2009 (see Fig. 5). The most obvious effect is a reversal in dune asymmetry along segments of the dunes where the September brinklines have retrograded to the NW from the brinkline positions in January. This reversal, which characterizes only the crestal portions of the dunes, results in small reversed slipfaces on the greater stoss slopes and is commonly referred to as "Chinese walls" (Fig. 14). Note that where the brinklines were roughly longitudinal to the wind resultant, Chinese walls did not occur, but rather these formed where the resultant was oblique or transverse to the brinklines, such that the former lee faces became temporary stoss slopes. In terms of dune deformation, however, the effects of the SSE winds are ephemeral. Because Figure 13 is a difference map, it shows differences in deposition and erosion between January 2009 and September 2009, a period that was largely dominated by the SW winds (see Fig. 5). Although brinkline tracing shows the retrogradation of the brinklines in the areas of the Chinese walls, which would have been accompanied by lee-face erosion and depositional build-up of the Chinese walls, it is the SW wind deposition/erosion signature that dominates the difference map. Restated, deposition/erosion that occurred with the SSE winds was less than deposition/erosion that occurred previously with the SW winds. Moreover, in comparing of the effects of the NNW and SSE winds modes (which are 180° apart, Fig. 4) on dune deformation, the sand-transporting potential of the NNW winds is significantly greater than that of the SSE winds (Fig. 8).

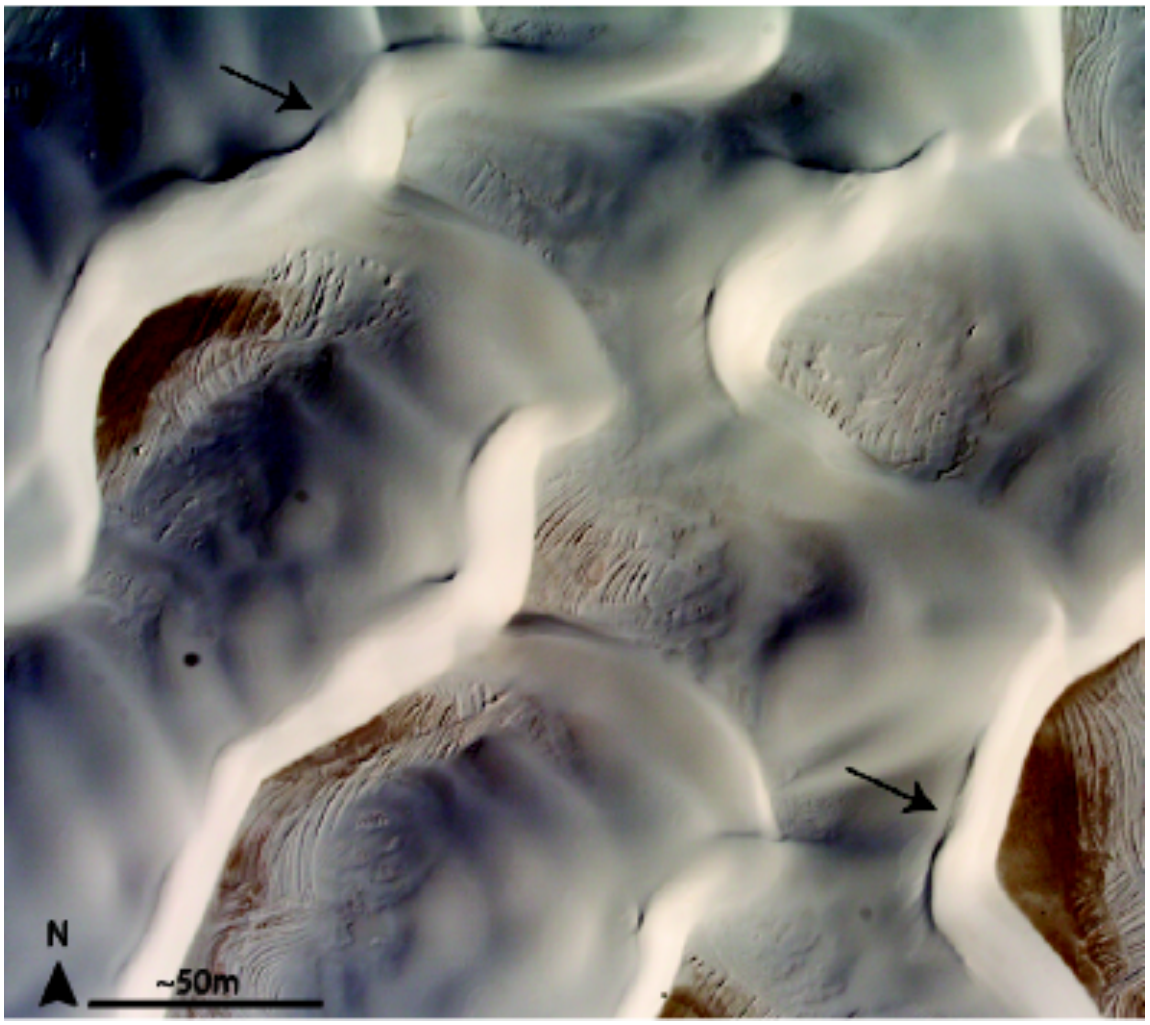

Figure 14. Aerial image of crescentic dunes with local crestal reversed slipfaces (arrows), referred to as “Chinese walls”. These features form with winds from the SSE mode.

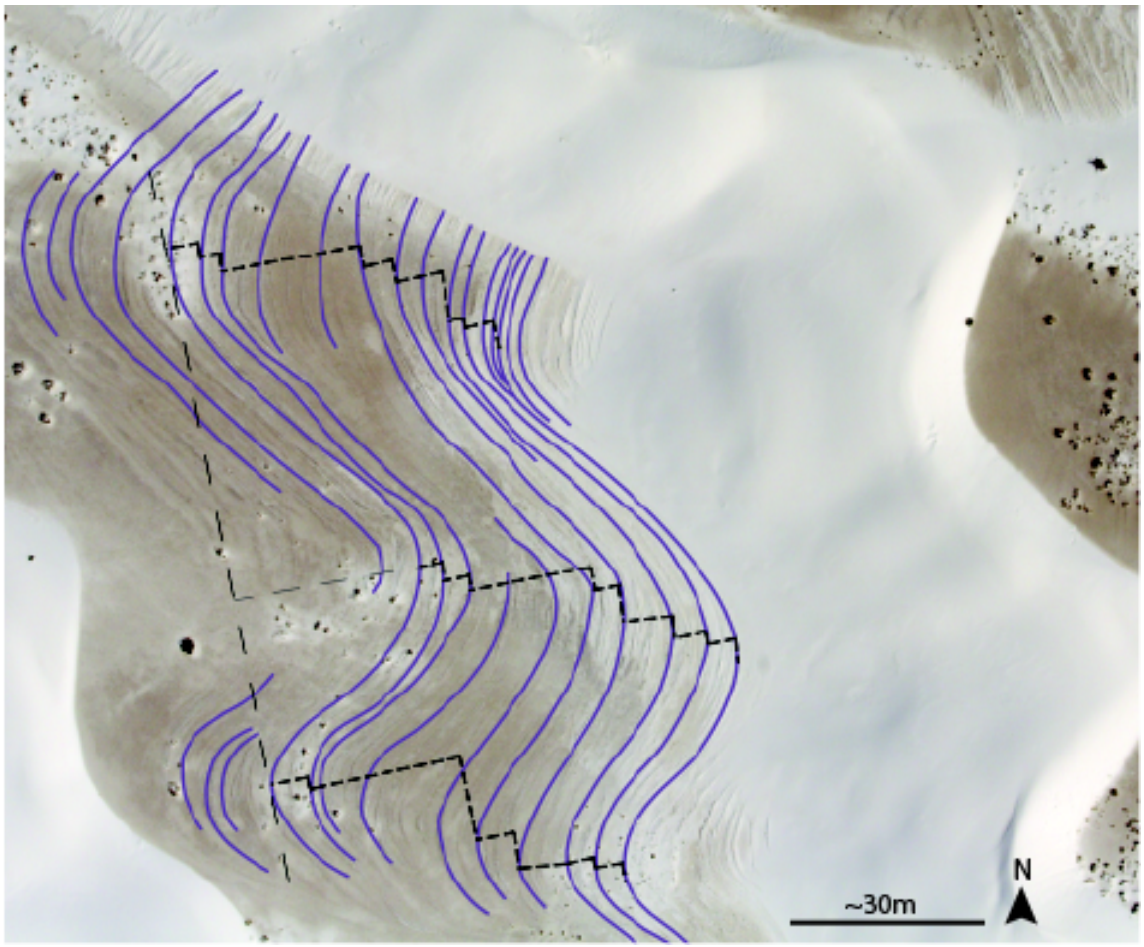

Figure 15. Plan-view cross-strata exposed in deflated interdune area. Raised cross-strata ridges allow for tracing of the migration of concave- and convex-downwind dune segments. Dashed line connecting centers of concave segments defines dune crestline orientation. Crest-normal and along-crest migration steps are mapped for continuous traces of cross-strata. Note that the steps are not uniform, indicating that the curving segments changed in shape as they migrated. Cross-strata readily traces into morphology of the current dune.

Whereas the lidar surveys provide only a three-year window into dune migration and deformation at White Sands, plan-view cross-strata exposed in deflated interdune areas provide a decadal record, as seen in low-altitude aerial photos (Fig. 15). The cross-

strata consists of two concave segments separated by a convex nose, and these segments readily can be projected into the current dune morphology (i.e., the cross-strata are the accumulations of the present-day dune). Where cross-strata ridges are continuous, these were traced as time-lies that approximate paleo-brinklines shapes. For the continuous traces, steps of crest-normal and along-crest migration are plotted (Fig.15). The ratios between along-crest and crest-normal migration are not uniform, ranging from 0.08 – 1.5 with a mean of 0.6 for the concave segments, and 0.25 – 1.4 with a mean of 0.7 for the convex segments. These differences result from differences in the wind regime over time, especially the sand-transporting capacity of the NNW winds. While migrating, therefore, the shape of the concave and convex segments also changed (i.e., deformed). The overall crescentic dune behavior at White Sands of forward migration with along-crest migration (crabbing) of the sinuosity is approximated by the model results of Rubin (1987, fig. 42), albeit that the shape of the sinuosity in the model is unchanging.

4.3 WHITE SANDS DUNE MODEL

4.3.1 Model Basis

The basis for model construction is that the rate of deposition/erosion of the lee face and its associated migration of the brinkline is both given by an analytic model (Rubin and Hunter, 1985) and field documentation during wind events at White Sands (Eastwood et al., 2012). The distribution of lee-face surface processes and resultant stratification types on a sinuous dune for a given wind direction is also presented by Eastwood et al. (2012). Dune deformation with migration and a spatially varying

distribution of surface processes arise from the dynamics created by the incidence angle formed between the primary wind and the local brinkline orientation. Dune dynamics as a function of incidence angle satisfactorily explains both dune behavior overall and during components of the wind regime (Section 4.2).

In the Rubin and Hunter (1985) analysis, sand transported over the brinkline and onto the lee face is decomposed into brinkline-normal and brinkline-parallel components of transport using a sine function of the incidence angle, $\propto$. Deposition is greatest where the wind is normal (transverse) to the brinkline and decreases with the incidence angle such that only brinkline-parallel transport occurs on the lee face where the wind and the brinkline are parallel (longitudinal). Only components of brinkline-normal deposition contribute to the forward migration of the lee face. In a field study at White Sands, Eastwood et al. (2012) confirmed the Rubin and Hunter (1985) analysis, but found that local deposition, ϕ, including lee-face erosion at low incidence angles, was best represented by

$$\phi = \sin(\alpha - 12^{\circ}). \quad (4)$$

Eastwood et al. (2012) also found that lee-face surface processes varied as a function of the local incidence angle, and conversely, the spatial distribution of stratification types along a set of cross-strata could be used to reconstruct the paleo-wind regime. Dune lee-face surface processes (and resultant stratification types) were first comprehensively described by Hunter (1977) as: (1) grainflow or avalanching (grainflow cross-strata), (2) grainfall (grainfall strata) where grains blown over the brinkline fall to

the surface and may build to the angle of initial yield and subsequently avalanche, and (3) wind ripples (wind-ripple laminae). Both grainflow and grainfall are gravity-driven processes, whereas wind ripples represent tractional transport. Based upon the White Sands data, a general characterization is that a lee face with: (1) grainflow and grainfall only reflect transverse incidence angles of 70° – 90°, (2) grainflow yielding downslope to wind ripples reflect high oblique incidence angles of 40° – 70°, (3) wind ripples only reflect low oblique incidence angles of 25° – 40°, (4) wind ripples without deposition (i.e., bypass surface) reflect incidence angles of 15° – 25°, and (5) wind ripples with net erosion (i.e., erosional surface) reflect incidence angles of 0° – 15° or an actual flow reversal.

Aspects of both lee-face deposition/erosion rates and the distribution of surface processes as a function of the incidence angle follow from the nature of secondary flow on the lee face (Allen, 1982; Sweet and Kocurek, 1990; Frank and Kocurek, 1996; Walker and Nickling, 2003). Lee-face wind speed has also been shown to be cosine function of the incidence angle, approaching zero at a transverse incidence angle and approaching the primary wind speed where the incidence angle is longitudinal (Tsoar, 1983; Sweet and Kocurek, 1990). For steep dunes (i.e., dunes with a slipface), at transverse incidence angles the secondary lee-face flow is largely a 2-D roller (back-eddy) with low wind speeds such that gravity-driven processes (grainflow and grainfall) dominate. As the incidence angle decreases (high oblique angles), a vortex forms with components of reversed and along-slope transport such that gravity-driven processes dominate on the upper slipface where depositional rates are highest, but these yield

downslope to wind ripples where lower rates of grainfall allow for dominance by tractional reworking. Tractional processes dominant at yet lower incidence angles and all sand passing over the brinkline is reworked into wind ripples, but rates of deposition continue to decrease with the incidence angle. Wind-ripple surfaces, therefore, may be depositional (i.e., positive angle of climb), bypassing (i.e., zero angle of climb) or erosional (i.e., negative angle of climb). A full review of lee-face processes is given in Eastwood et al. (2012).

4.3.2 Model

Based upon the analysis given above (Section 4.3.1), overall dune behavior during the three-year study period and specific deformation associated with a wind mode can be described in a generalized model (Fig. 16). The dune shape used in Figure 16 is typical of dunes at White Sands, but because the model is based upon incidence angle, specific results will vary with dune shape. Moreover, a near compass-wide span of winds occur at White Sands (Fig. 4) and each wind direction will form an incidence angle with a given brinkline segment. Modeled here are wind directions taken as the resultants from the three wind modes at White Sands (Fig. 4).

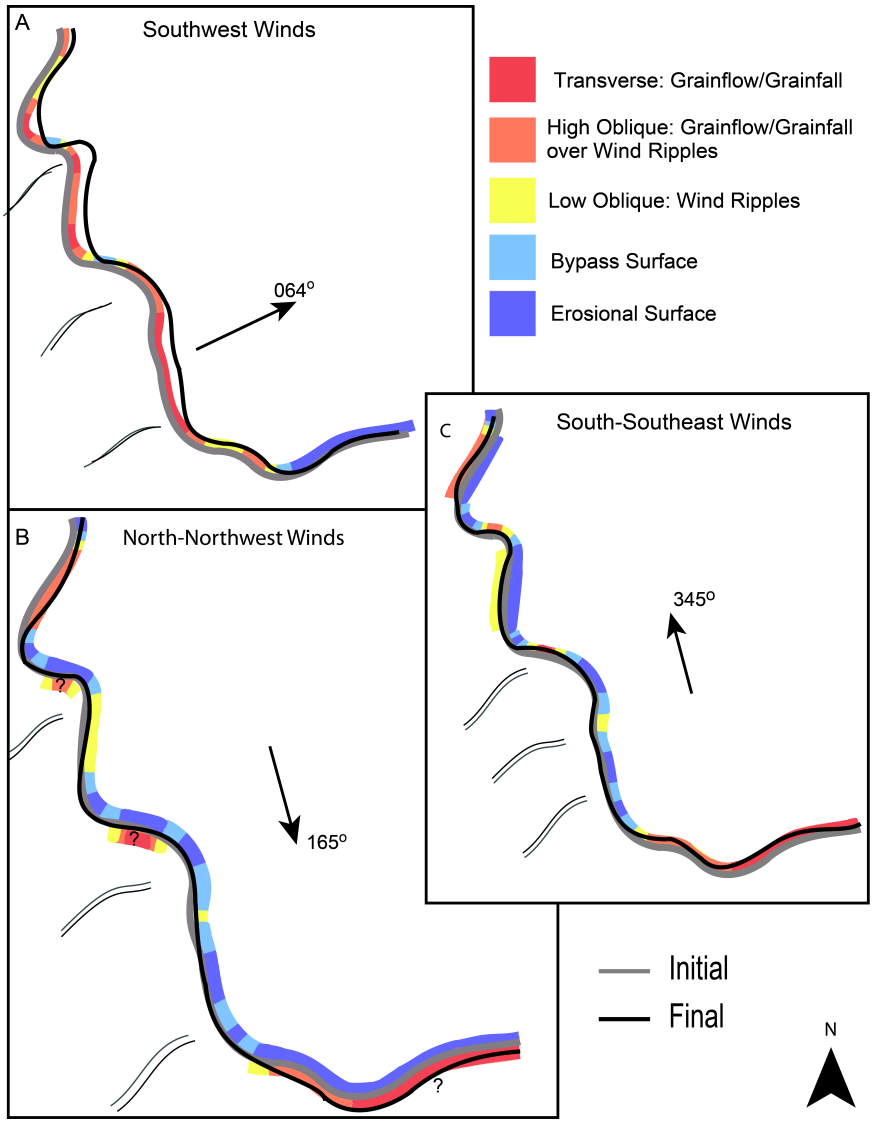

Figure 16. Model for sinuous dune migration, deformation and surface processes (stratification types) based upon incidence angles for the resultant for the three wind modes. (A) SW winds, which cause most dune migration and grainflow/grainfall lee face. Departures occur at local low incidence angles along flanks of convex noses and dune terminations. (B) NNW winds, which give rise to along-crest migration of sinuosity, and SE migration of stoss bedforms and NE-trending dune terminations. Much of dune lee face is characterized by bypass or erosional surface, which creates a bounding surface. (C) SSE winds, which give rise to ephemeral crest reversals (Chinese walls), NW migration of stoss bedforms, and dune terminations.

Figure 16A characterizes dune behavior with the dominant SW winds. Because the dunes are generally transverse to this wind and the SW winds are the dominant sand-transporting winds, the greatest dune migration occurs. Greatest migration occurs along transverse dune segments, were the lee faces are characterized by grainflow and grainfall surface processes. Dune sinuosity, however, also gives rise to weakly oblique dune segments (grainflow/grainfall over wind ripples), and very oblique segments (wind ripples) with correspondingly lower rates of dune migration. Bypass and even erosional dune lee-face segments can occur with the SW winds, but these low incidence angles largely characterize some flanks of convex-downwind noses and dune terminations. Superimposed stoss bedforms, oriented normal to the brinkline, are largely longitudinal elements for the SW winds and do not migrate. Overall, note that although the dunes are nearly transverse to the SW wind resultant, dune deformation does occur because the dunes are sinuous, and surface processes vary along the lee face as a function of local incidence angle.

Figure 16B characterizes dune behavior with the NNW winds. Although these winds are minor in comparison to the SW winds in sand-transporting capacity, because the NNW winds are nearly parallel to the dune trend, significant dune deformation occurs, which is then not reworked by the SW winds. The primary effects of the NNW winds are: (1) along-crest migration of the dune sinuosity with an erosional bounding surface created on the NW flanks of the sinuosity and deposition on the SE flanks, (2) SE migration with slipface development on NE-trending dune terminations, and (3) SE migration of stoss superimposed dunes. During the NNW winds long segments of the

dune are bypass or erosional surfaces, which should be manifested within sets of cross-strata as bounding surfaces. Although local brinkline segments are oriented nearly transverse to the NNW winds and local crestal reversals are forecast, at least in our experience these are uncommon. This may reflect the fact that NNW winds, at least those associated with frontal passage, are short duration events rapidly modified by the dominant SW winds.

Figure 16C characterizes dune behavior with the weak SSE winds. In comparison to the effects of the NNW winds (Fig. 16B), NE-trending dune terminations reverse asymmetry and may migrate to the NW, wind-ripple migration direction is reversed on bypass and erosional surfaces, superimposed stoss bedforms migrate to the NW, and local crestal reversals occur (Chinese walls). Unlike the NNW winds, however, the difference map for this wind (Section 4.2) shows that the impact of the SSE winds is reworked by the SW and NNW winds. The primary stratigraphic effect will be erosional bounding surfaces created on the lee faces where flow is reversed and Chinese walls are created.

4.4 Predicting Dune Migration and Deformation

Based upon measured deposition/erosion on lee faces during single wind events at White Sands, Eastwood et al. (2012, fig. 7) found a correlation of $r^2 = 0.53$ between the normalized deposition/erosion rate and local incidence angle, which was taken as a relatively strong correlation given a "noisy" natural system. Figure 17 plots incidence angle using the 2007 brinklines against migration rate for dune segments discretized in the 24 dunes selected for detailed analysis (Fig. 3). A trend is apparent but

the correlation falls to $r^2 = 0.28$ for this three-year period. It is predicted that this correlation would continue to decrease with time as the dunes increasingly depart from their original June 2007 shape. For a sinuous dune to perfectly maintain its shape, each point in Figure 17 would have to migrate the same distance and the line would have zero slope. In effect, the trend reflects the degree of deformation of the dunes over time, which results from unequal deposition/erosion rates along the lee face as a function of the local incidence angles.

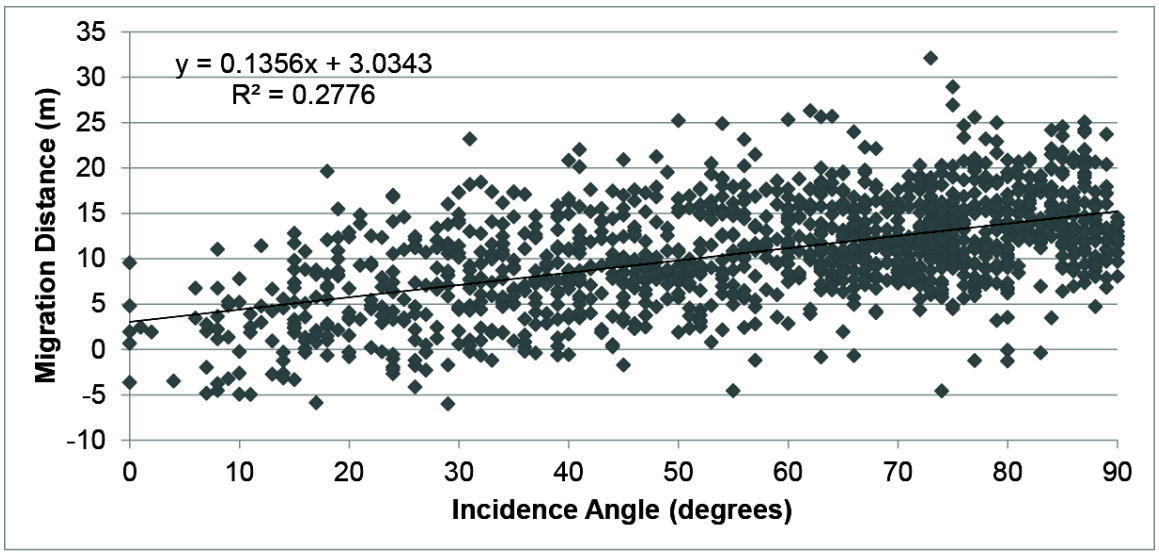

Figure 17. Plot of local incidence angles for straight-line dune segments defined by points for 24 discretized dunes (Fig. 3) against migration distance between 2007 and 2010 DEMs. Although a trend is apparent such that migration increases with incidence angle, the correlation is low.

As apparent from actual (Section 4.2) and idealized (Section 4.3.2) dune behavior, dunes deform with each wind event to, typically, some small degree. The new dune shape is then the boundary condition for the next wind events and yet additional dune deformation occurs. For perfectly straight-crested dunes no dune deformation would

occur regardless of changes in wind direction because components of crest-normal and crest-parallel transport would be the same everywhere on the lee face. For sinuous dunes, where local deposition/erosion is a function of the local incidence angle, deformation must occur. In the long-term where the wind regime is not changing overall, dunes assume a gross bedform-normal orientation (Rubin and Hunter, 1987), but as evident from Figure 5, the monthly wind regime is not the same year-to-year and the single year resultants are not the same. In terms of questions advanced in the introduction (Section 1), exact sinuous dune shape cannot be predicted from the wind resultant and an initial dune shape. Rather, the dunes are behaving as complex systems where every wind incrementally deforms the dune, which, in turn, then defines the beginning dune shape for the next wind event. The attractor for the system, where long-term boundary conditions are not changing, is defined by crestline orientation (Werner, 2003), as measured by the gross bedform-normal orientation (Rubin & Hunter, 1987), overall dune type (e.g., crescentic), and gross deformation such as along-brinkline migration of sinuosity. Predicting dune shape from and original form becomes incresingly inaccurate with time.

5. Conclusions

Synthesis of wind data collected at Holloman AFB for the period of June 2007 – June 2010 into sand-transporting events allows for a realistic characterization of the wind regime at White Sands. Identification of the strongly dominant SW wind mode, lesser wind modes from the NNW and SSE, and a net resultant toward 065° agree with previous work, but monthly analysis of the winds shows that the previous seasonal characterization is oversimplified. The wind regime is characterized by spring (March – May) strong SW winds with the longest wind-event durations. Wind directions during the remainder of the year are far more variable. Moreover, wind resultants calculated on an annual basis differ from the long-term resultant. Calm days significantly out number days with winds above threshold speed. About 80 sand-transporting events happen on average each year, and while most last for a few hours, less common wind events may last for days. This study agrees with Jerolmack and Brzinski (2010) that the most constructive wind at White Sands in terms of the combination of frequency and magnitude has a $u_* = 0.39$ m/s, and these winds are mostly associated with the SW winds.

Comparison of the wind record to overall dune behavior and dune behavior to the three modes of the wind regime was based upon a time series of five airborne lidar-derived DEMs. Overall dune behavior consists of approximately crestline-normal migration, and along-crest migration of dune sinuosity as well as low bedforms superimposed on the stoss slope to the SE. Because of dune sinuosity, brinkline advance is not uniform and the dune deform with migration. The SW winds are responsible for most forward migration, whereas the NNW winds cause along-crest migration of the

sinuosity, and the SSE winds cause ephemeral crestal reversal. Dune behavior can be satisfactorily explained as a function of the incidence angle formed between the primary wind direction and the local orientation of the brinkline. An idealized model characterizes dune migration with deformation according to incidence angle, and predicts the distribution of surface processes along the lee-face following from field documentation by Eastwood et al. (2012).

The dunes at White Sands behave as complex systems. Beginning with an initial dune shape, future dune shape is forecast with decreasing reliability with increasing time. Each wind event deforms the dunes to some small degree because rates of deposition and erosion are not uniform along the lee face. The dune shape after a wind event is not only slightly different from the shape before the event, the new shape defines the initial configuration for the next wind event. In complex-systems terminology, variable winds events and other boundary conditions at White Sands (Ewing and Kocurek, 2010b) define the variables that give rise to the phase space of the attractor that is the White Sands dune-field pattern. The attractor defines the crescentic dune type, the gross bedform-normal dune orientation, and large-scale deformation such as along-crest migration of the sinuosity. Specific dune shape varies within the limits of the phase space, but is not exactly predictable at a given time (c.f., Werner, 2003).

References

Allen JRL. 1982. Sedimentary Structures: Their Character and Physical Basis: 2. Elsevier Science Publishers: Amsterdam

Baitis E, Kocurek G, Smith V, Mohrig D, Ewing RC, Peyret A-PB. 2014. Definition and Origin of the Dune-Field Pattern at White Sands, New Mexico. *Aeolian Research*. DOI: 10.1016/j.aeolia.2014.06.004

Eastwood EN, Kocurek G, Mohrig D, Swanson T. 2012. Methodology for reconstructing wind direction, wind speed and duration of wind events from aeolian cross-strata. *Journal of Geophysical Research* **117**(F3), F03035. doi:10.1029/2012JF002368

Elbelrhiti HP, Claudin P, Andreotti B. 2005. Field evidence for surface-wave-induced instability of sand dunes. *Nature* **437**: 720-723. doi:10.1038/nature04058

Ewing RC, Kocurek G, Lake L. 2006. Pattern analysis of dune-field parameters. *Earth Surface Processes and Landforms* **31**: 1176-1191.

Ewing RC, Kocurek G. 2010a. Aeolian dune interactions and dune-field pattern formation: White Sands Dune Field, New Mexico. *Sedimentology* **57**: 1199-1219.

Ewing RC, Kocurek G. 2010b. Aeolian dune-field pattern boundary conditions. *Geomorphology* **114**(3): 175–187. doi:10.1016/j.geomorph.2009.06.015

Fryberger SG. 2003. Geological overview of White Sands National Monument. Available from http://www.nature.nps.gov/geology/parks/.

Frank A, Kocurek G. 1996. Toward a model for airflow on the lee side of aeolian dunes. *Sedimentology* **43**: 451-458.

Génois M, du Pont SC, Hersen P, Grégoire G. 2013. An agent-based model of dune interactions produces emergence of patterns in deserts. *Geophysical Research Letters* **40**, 3909-3914. doi:10.1002/grl.50757

Hersen P, Douady S. 2005. Collision of barchan dunes as a mechanism of size regulation. *Geophysical Research Letters* **32**(21). doi:10.1029/2005GL024179

Hunter RE, Richmond BM, Alpha TR. 1983. Storm-controlled oblique dunes of the Oregon coast. *Geological Society of America Bulletin* **94**: 1450–1465.

Iversen JD, White BR. 1982. Saltation threshold on Earth, Mars and Venus. *Sedimentology* **29**: 111–119.

Kawamura R. 1951. Study of sand movement by wind. Hydraulic Engineering Report HEL-2–8, Univ. of California, Berkeley.

Jerolmack DJ, Brzinski Ta. 2010. Equivalence of abrupt grain-size transitions in alluvial rivers and eolian sand seas: A hypothesis. *Geology* **38**(8): 719–722. doi:10.1130/G30922.1

Jerolmack DJ, Reitz MD, Martin RL. 2011. Sorting out abrasion in a gypsum dune field. *Journal of Geophysical Research* **116**(F2), F02003. doi:10.1029/2010JF001821

Jerolmack DJ, Ewing RC, Falcini F, Martin RL, Masteller C, Phillips C, Reitz MD, Buynevich I. 2012. Internal boundary layer model for the evolution of desert dune fields. *Nature Geoscience* **5**: 206-209.

Kocurek G, Ewing RC. 2005. Aeolian dune field self-organization – implications for the formation of simple versus complex dune-field patterns. *Geomorphology* **72**: 94-105.

Kocurek G, Carr M, Ewing R, Havholm KG, Nagar YC, Singhvi aK. 2007. White Sands Dune Field, New Mexico: Age, dune dynamics and recent accumulations. *Sedimentary Geology* **197**(3-4): 313–331. doi:10.1016

Kocurek G, Ewing RC, Mohrig D. 2010. How do bedform patterns arise? New views on the role of bedform interactions within a set of boundary conditions. *Earth Surface Processes and Landforms* **35**: 51–63. doi:10.1002/esp

Langford RP, Rose JM, White DE. 2009. Groundwater salinity as a control on development of eolian landscape: An example from the White Sands of New Mexico. *Geomorphology* **105**: 39–49.

Langford RP. 2003. The Holocene history of the White Sands dune field and influences on eolian deflation and playa lakes. *Quaternary International*: **104**(1): 31–39. doi:10.1016/S1040-6182(02)00133-7

McKee ED. 1966. Structures of dunes at White Sands National Monument, New Mexico (and a comparison with structures of dune from other selected areas). *Sedimentology* **7**: 3–69. doi:10.1111/j.1365-3091.1966.tb01579

Namikas S, Sherman DJ. 1997. Predicting aeolian sand transport: Revisiting the White model. *Earth Surface Processes and Landforms* **22**: 601–604.

Rachal, DM, Dugas DP. 2009. Historical dune pattern dynamics: White Sands Dune Field, New Mexico. *Physical Geography* **30**: 64-78.

Rubin DM, Hunter RE. 1985. Why deposits of longitudinal dunes are rarely recognized in the geologic record. *Sedimentology* **32**: 147–157.

Rubin D M, Hunter RE. 1987. Bedform alignment in directionally varying flows. *Science* **237**(4812): 276–8. doi:10.1126/science.237.4812.276

Rubin D M 1987. Concepts in Sedimentology and Paleontology, vol. 1, Cross-bedding, Bedforms, and Paleocurrents, SEPM, Tulsa, Okla., http://dx.doi.org/10.2110/csp.87.01, doi:10.2110/csp.87.01.

Shao Y, Lu H. 2000. A simple expression for wind erosion threshold friction velocity. *Journal of Geophysical Research* **105**(D17): 22437–22443. doi:10.1029/2000JD900304

Sweet ML, Kocurek G. 1990. An empirical model of aeolian dune lee-face air-flow. *Sedimentology* **37**: 1023–1038.

Tsoar H. 1983. Dynamic processes acting on a longitudinal (seif) sand dune. *Sedimentology* **30**: 567–578.

Walker IJ, Nickling WG. 2003. Dynamics of secondary airflow and sediment transport over and in the lee of transverse dunes. *Progress Physical Geography* **26**: 47–75.

Werner BT. 1999. Complexity in natural landform patterns. *Science* **284**: 102-104.

Werner BT. 1995. Eolian dunes: computer simulations and attractor interpretation. *Geology* **23:** 1107–1110.

White, BR .1979. Soil transport by wind on Mars. *Journal of Geophysical Research* **84**: 4643–4651.

Wolman MG, Miller JP. 1960. Magnitude and Frequency of Forces in Geomorphic Processes. *The Journal of Geology* **68**(1): 54–74. doi:10.2307/30058255